Accepted Manuscript

Synthesis and structure-activity relationships of quinolinone and quinoline-based P2X7 receptor antagonists and their anti-sphere formation activities at glioblastoma cells

Seung-Hwa Kwak, Seungheon Shin, Ji-Hyun Lee, Jin-Kyoung Shim, Minjeong Kim, So-Deok Lee, Aram Lee, Jinsu Bae, Jin-Hee Park, Aliaa Abdelrahman, Christa E. Müller, Steve K. Cho, Seok-Gu Kang, Myung Ae Bae, Jung Yoon Yang, Hyojin Ko, Yong-Chul Kim

PII: S0223-5234(18)30266-6

DOI: 10.1016/j.ejmech.2018.03.023

Reference: EJMECH 10288

To appear in: *European Journal of Medicinal Chemistry*

Received Date: 21 September 2017

Revised Date: 28 February 2018

Accepted Date: 8 March 2018

Please cite this article as: S.-H. Kwak, S. Shin, J.-H. Lee, J.-K. Shim, M. Kim, S.-D. Lee, A. Lee, J. Bae, J.-H. Park, A. Abdelrahman, C.E. Müller, S.K. Cho, S.-G. Kang, M.A. Bae, J.Y. Yang, H. Ko, Y.-C. Kim, Synthesis and structure-activity relationships of quinolinone and quinoline-based P2X7 receptor antagonists and their anti-sphere formation activities at glioblastoma cells, *European Journal of Medicinal Chemistry* (2018), doi: 10.1016/j.ejmech.2018.03.023.

Graphical Abstract

To create your abstract, type over the instructions in the template box below.
Fonts or abstract dimensions should not be changed or altered.

Synthesis and Structure-Activity Relationships of Quinolinone and Quinoline-based P2X7 Receptor Antagonists and their Anti-sphere Formation Activities at Glioblastoma Cells

Leave this area blank for abstract info.

Seung-Hwa Kwak[a,#], Seungheon Shin[b], Ji-Hyun Lee[c], Jin-Kyoung Shim[c], Minjeong Kim[a,†], So-Deok Lee[a], Aram Lee[a], Jinsu Bae[b], Jin-Hee Park[a,^], Aliaa Abdelrahman[d], Christa E. Müller[d], Steve K. Cho[a,b], Seok-Gu Kang[c], Myung Ae Bae[e], Jung Yoon Yang[e], Hyojin Ko[a*] and Yong-Chul Kim[a,b*]

[a]School of Life Sciences, Gwangju Institute of Science and Technology (GIST), Gwangju 500-712, Republic of Korea. [b]Department of BioMedical Science and Engineering (BMSE), Gwangju Institute of Science and Technology (GIST), Gwangju 500-712, Republic of Korea. [c]Department of Neurosurgery, Brain Tumor Center, Severance Hospital, Yonsei University College of Medicine, Seoul 03722, Republic of Korea. [d]PharmaCenter Bonn, Pharmaceutical Institute, Pharmaceutical Chemistry I, University of Bonn, An der Immenburg 4, D-53121 Bonn, Germany. [e]Bio & Drug Discovery Division, Korea Research Institute of Chemical Technology (KRICT), Daejeon 34114, Republic of Korea

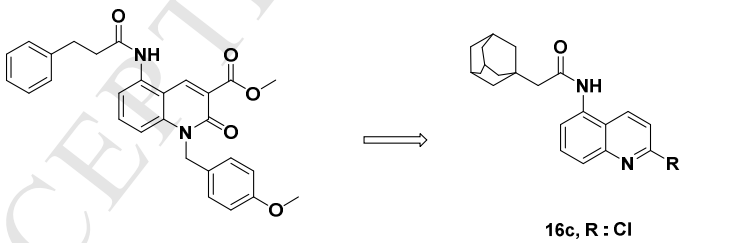

11a
(EtBr 50% inhibition at 10 μM)

16c, R : Cl
(EtBr IC_{50} = 4 nM, IL-1β IC_{50} = 7 nM

17k, R : Ph-(4-CH_2OH)
(EtBr IC_{50} = 3 nM, IL-1β IC_{50} = 12 nM

Synthesis and Structure-Activity Relationships of Quinolinone and Quinoline-based P2X7 Receptor Antagonists and their Anti-sphere Formation Activities in Glioblastoma Cells

Seung-Hwa Kwak[a,#], Seungheon Shin[b], Ji-Hyun Lee[c], Jin-Kyoung Shim[c], Minjeong Kim[a,†], So-Deok Lee[a], Aram Lee[a], Jinsu Bae[b], Jin-Hee Park[a,^], Aliaa Abdelrahman[d], Christa E. Müller[d], Steve K. Cho[a,b], Seok-Gu Kang[c], Myung Ae Bae[e], Jung Yoon Yang[e], Hyojin Ko[a*] and Yong-Chul Kim[a,b*]

[a]School of Life Sciences, Gwangju Institute of Science and Technology (GIST), Gwangju 500-712, Republic of Korea.

[b]Department of BioMedical Science and Engineering (BMSE), Gwangju Institute of Science and Technology (GIST), Gwangju 500-712, Republic of Korea.

[c]Department of Neurosurgery, Brain Tumor Center, Severance Hospital, Yonsei University College of Medicine, Seoul 03722, Republic of Korea.

[d]PharmaCenter Bonn, Pharmaceutical Institute, Pharmaceutical Chemistry I, University of Bonn, An der Immenburg 4, D-53121 Bonn, Germany.

[e]Bio & Drug Discovery Division, Korea Research Institute of Chemical Technology (KRICT), Daejeon 34114, Republic of Korea

*Corresponding Author: Prof. Hyojin Ko and Prof. Yong-Chul Kim. Tel: +82-62-715-2502; Fax: +82-62-715-2484. Email address: kohyojin@gist.ac.kr (H. J. Ko); yongchul@gist.ac.kr (Y.- C. Kim).

Present address: Department of Chemistry, Duke University, Durham, North Carolina 27708, United States.

† Present address: COSMAX, #701, Pangyo inno valley E, 255, Pangyo-ro, Bundang-gu, Seongnam-si, Gyeonggi-do, Republic of Korea.

^ Present address: New Drug Development Center (NDDC), Daegu-Gyeongbuk, Medical Innovation

Foundation (DGMIF), 80 Cheombok-ro, Dong-gu, Daegu 41061, Republic of Korea.

ABSTRACT

Screening a compound library of quinolinone derivatives identified compound **11a** as a new P2X7 receptor antagonist. To optimize its activity, we assessed structure-activity relationships (SAR) at three different positions, R_1, R_2 and R_3, of the quinolinone scaffold. SAR analysis suggested that a carboxylic acid ethyl ester group at the R_1 position, an adamantyl carboxamide group at R_2 and a 4-methoxy substitution at the R_3 position are the best substituents for the antagonism of P2X7R activity. However, since most of the quinolinone derivatives showed low inhibitory effects in an IL-1β ELISA assay, the core structure was further modified to a quinoline skeleton with chloride or substituted phenyl groups. The optimized antagonists with the quinoline scaffold included 2-chloro-5-adamantyl-quinoline derivative (**16c**) and 2-(4-hydroxymethylphenyl)-5-adamantyl-quinoline derivative (**17k**), with IC_{50} values of 4 and 3 nM, respectively. In contrast to the quinolinone derivatives, the antagonistic effects of the quinoline compounds (**16c** and **17k**) were paralleled by their ability to inhibit the release of the pro-inflammatory cytokine, IL-1β, from LPS/IFN-γ/BzATP-stimulated THP-1 cells (IC_{50} of 7 and 12 nM, respectively). In addition, potent P2X7R antagonists significantly inhibited the sphere size of TS15-88 glioblastoma cells.

Keywords: P2X7 receptor, antagonist, IL-1β, EtBr, inflammation, quinoline, quinolinone, anti-glioma

1. Introduction

Purinergic receptors are plasma membrane proteins that can be classified into three different families: P1, P2X and P2Y. Broadly, P1 (adenosine) and P2Y receptors are G protein-coupled receptors (GPCR), and the P2X receptors are ligand-gated ion channels that are activated by extracellular ATP molecules.[1-4]

In the case of P2X receptors (P2XR), seven different subtypes, P2X1–P2X7, have been identified in the immune and nervous systems. Among the P2XR subtypes, P2X7R has drawn particular interest in terms of its distinctive molecular structure, such as a longer C-terminus with 100-200 amino acids and pathological functions related to inflammation. In the tertiary structure of the ion channel, P2X7R is composed of homotrimeric subunits, and the receptor is mainly expressed in hematopoietic cells, including mast cells, lymphocytes, erythrocytes, and macrophages.[5] The P2X7Rs also play important pathophysiological functions in the human monocyte cell line THP-1, epidermal Langerhans cells, fibroblasts, and cells in the central nervous system (CNS) such as microglia and Schwann cells, which suggests that the receptor is involved in diseases such as chronic inflammation, neurodegeneration, and chronic pain.[6]

P2X7R is activated not only by the endogenous ligand ATP but also by other agonists such as BzATP, ADP, UTP and AMP.[3,7,8] As a unique function of the receptor, the activation of P2X7R results in the formation of permeable pores and the induction of signaling cascades downstream of the receptor. Upon the activation of P2X7R, cations such as Ca^{2+}, Na^{+} and K^{+} can be permeable through the ion channel or pore. This process leads to the activation of related inflammatory signals, including phospholiphase A2, phospholiphase D, mitogen-activated protein kinase (MAPK), and nuclear factor kappa-light-chain-enhancer of activated B cells (NF-κB).[9] More importantly, P2X7R activation ultimately stimulates the release of

interleukin-1β (IL-1β),[10,11] which is a master cytokine for the mediation of inflammatory signals, along with cell proliferation, differentiation and apoptosis.[12] In addition, P2X7R triggers several other signaling cascades, which ultimately lead to macrophage fusion, superoxide production in microglia and lymphoid cells.[13,14] Thus, therapeutic interventions targeting P2X7R have been explored as a novel approach for the prevention or treatment of inflammatory disorders such as arthritis, chronic inflammatory pain, neuropathic pain, and neurodegenerative diseases.[15-18] In addition, P2X7R is over-expressed in various cancer cells, in which it has been reported to show important functions, such as improved survival, invasiveness, and metastasis, in cancer microenviroments.[19,20] Recently, P2X7R was reported to be involved in the activation of microglia located near glioma cells.[21] The inhibition of P2X7R function showed a decrease in the number of glioma cells, which can induce glioblastoma. Glioblastoma is the most common type of brain tumor and a major cause of their high morbidity.[22]

According to the above diverse pathophysiological functions of the P2X7 receptor, several P2X7R antagonists have been discovered. For example, KN-62 (**1**, Figure 1), previously known as a type II Ca^{2+}/calmodulin-dependent kinase inhibitor, was developed as an early-generation P2X7R antagonist.[23] The antagonists developed by the pharmaceutical industry for the purpose of new drug discovery are compounds **2**–**5** in Figure 1. AZD9056 (**2**) is an orally bioavailable P2X7R antagonist with an IC_{50} value of 10-13 nM (IL-1β ELISA assay), targeting rheumatoid arthritis (RA), chronic obstructive pulmonary disease (COPD) and Crohn's disease. However, compound **2** failed in phase 2 clinical trials because it did not show appreciable efficacy compared with placebo.[24] Another potent and highly selective P2X7R antagonist, CE-224535 (**3**), also entered clinical trials for treating patients with RA that was inadequately controlled by methotrexate, but it failed to show significant efficacy.[25] A-438079 (**4**) and GSK314181A (**5**) were reported to have anti-nociceptive effects in

neuropathic[26] and inflammatory pain[27,28] and are currently in the discovery stage.

We have reported diverse classes of P2X7R antagonists, including dichloropyridine (**6**),[29] and 2,5-dioxoimidazolidine derivatives (**7**).[30] Recently, we reported potent imidazole-based P2X7R antagonists (**8**)[31] with significant anti-migration and invasion activities against metastatic breast cancers.

To discover new chemical entities as P2X7R antagonists, a quinolinone library[32] that was previously reported by our group was screened to identify a hit compound (**11a**, Table 1) as a weak P2X7R antagonist. The quinolinone scaffold has been studied extensively to develop agents for treating immune disorders.[33-36] Moreover, we recently reported the optimization of quinolinone derivatives for their inhibitory effects on IL-2 secretion and their functional mechanism of immunomodulation.[37] In this report, we describe the development of new P2X7R antagonists by structure-activity relationships (SAR) and the optimization of the quinolinone-based hit compound, **11a**. In addition, the functional effects of the representative compound, including the inhibition of IL-1β release, which is closely related to immune disorders, and anti-sphere formation activities against glioblastoma cells, in which P2X7 receptors are overexpressed and function as activation of microglia located near glioblastoma cells, were examined.[21, 22]

2. Results and discussion

2.1. Chemistry

The general synthetic procedures for the quinolinone and quinoline analogs are described in Schemes 1 and 2, and a full list of synthesized analogs is provided in Tables 1–5.

The starting materials, 5-nitroquinolin-2(1H)-one (**9a**)[38] and methyl 5-nitro-2-oxo-1,2-dihydroquinoline-3-carboxylate (**9b**),[32] were prepared following the previously reported procedure.[32,38] 5-Nitro groups of **9a**–**b** were first reduced to the corresponding amines with $SnCl_2$, and the amide moieties of the quinolinone skeletons were selectively reacted with appropriate benzyl chlorides or benzyl bromides to afford a series of compounds, **10a**–**l**. The amino group of compounds **10a**–**l** was subjected to acylation reactions with appropriate acid chlorides to afford **11a**–**i**, **12a**–**j** and **13a**. In this step, coupling reaction conditions with carboxylic acid moiety (R_2CO_2H) failed to yield the desired products. For the synthesis of **13b**–**g**, the methyl ester of **11i** was hydrolyzed under basic conditions using 10% KOH in MeOH to a carboxylic acid analogue, **13b**, which was subsequently subjected to coupling reactions with several alkyl amines, such as methylamine and dimethylamine, to produce **13f** and **13g** and with various alcohols to afford **13c**–**e** (Scheme 1).

The synthetic scheme for quinoline derivatives from the quinolinone structure is described in Scheme 2. The quinolinone amide groups of **9a** and **9b** were first converted into chloroquinoline moieties by reaction with $POCl_3$ (**14a** and **14b**). Then, the 5-nitro groups of **14a** and **14b** were reduced to the amine with $SnCl_2$ to afford compounds **15a** or **15b**, which were subjected to acylation reactions with appropriate acid chloride groups to produce **16a**–**e**. Next, for the introduction of diverse groups at the R_4 position, appropriate boronic acid derivatives were reacted with **16c** under Suzuki-Miyaura cross-coupling conditions to yield

17a–**g** and **17i**. Compound **17h** was obtained from the reduction of **17g** by using $SnCl_2$, and **17i** was further transformed into the corresponding ester analogue **17j** by methylation using CH_3I and was then subsequently reduced with LAH to afford **17k**.

2.2. Biology

2.2.1. Structure-Activity Relationships (SAR) To investigate the SAR of the quinolinone and quinoline derivatives, the P2X7R antagonistic activities of all of the synthesized compounds were evaluated using an ethidium bromide (EtBr) uptake assay in human HEK293 cells stably expressing *h*P2X7 receptors. KN-62 (**1**) and AZD9056 (**2**) were used as positive controls, for which the IC_{50} values (158 and 2 nM, respectively) were found to be similar to the reported data.[23,24]

As an initial SAR analysis, aryl moieties (**11a**–**c**), alkyl moieties (**11d**–**g**) and adamantyl moieties (**11h** and **11i**) with different carbon chain lengths were explored at the R_2 position because compound **10b** with no substituent at 5-amino group showed a complete loss of activity compared to the hit compound **11a** (Table 1). In the analysis of the effects of carbon chain lengths between phenyl and carbonyl groups of compounds **11a**–**c**, a longer carbon chain showed a profile of increased antagonistic effects. For cycloalkyl moieties (**11e**–**g**), the tendency of antagonistic activities related with the carbon chain lengths was opposite compared with aromatic moieties (**11a**–**c**). Thus, a decreased carbon chain length afforded a sharp increase in the antagonistic effects, as shown in the case of **11d**–**g**, with 15% and 20% inhibition at 1 μM (**11d** and **11e**, No. of carbon in chain: 2), 875 nM (**11f**, No. of carbon in chain: 1) and 810 nM (**11g**, No. of carbon in chain: 0). This profile of P2X7R antagonistic activities was also observed in the polycycloalkyl derivatives, **11h** and **11i**, which showed potent antagonistic effects with IC_{50} values of 861 and 120 nM, respectively. Based on this

result, we concluded that intact bulky cycloalkyl carboxamide groups substituted at the 5-position of the quinolinone structure is important for P2X7R antagonism.

Next, we investigated the SAR of R_3 substituents by modifications of the benzyl substituents to 3-methoxy (**12a**), halide (**12c**–**e**), alkyl (**12f**–**g**) and electron-withdrawing groups such as nitro (**12h**) and cyano (**12i**), respectively, while maintaining the R_2 position as adamantyl carboxamide (Table 2). Comparing **11i** and **12a**, changing the substituted position of the 4-methoxy group to the *meta* position resulted in a significantly decreased antagonistic effect. Thus, all other substituents were introduced at the *para* position of the benzyl moiety. The activity profile of the series of compounds was as follows: 4-ethyl (**12g**), 4-methyl (**12f**) < 4-trifluoro-methoxy (**12b**) < 4-fluoro (**12c**), 4-bromo (**12e**), 4-nitro (**12h**), 4-chloro (**12d**) < 4-methoxy (**11i**). Among the derivatives (**11i**, **12a**−**j**), the halide-substituted compounds (**12c**−**e**) and nitro (**12h**) showed IC_{50} values of 720−880 nM. The simple alkyl substituted derivatives with 4-methyl (**12g**) or 4-ethyl (**12f**) groups decreased the P2X7R antagonistic activity dramatically compared with other halide, nitro and alkoxy substituted analogs including the most active compound, **11i** with 4-methoxy group in Table 2. Basis on the results shown in Tables 1 and 2, adamantyl carboxamide at R_2 and 4-methoxybenzyl group at R_3 exhibited best outcome and were fixed for the further analysis of the SAR of R_1 substituents.

Thus, the methyl ester group at the R_1 position was modified to hydrogen, carboxylic acid, various alkyl esters (**13c**−**e**) and carboxamides (**13f** and **13g**) to investigate the possible effects of hydrogen bond acceptors or donors in this position. P2X7R antagonistic activity was lost upon the removal (**13a**) or hydrolysis (**13b**) of the methyl ester group of **11i**. The optimum alkyl moiety of the ester group was determined to be the two carbon ethyl moiety (**13c**), which displayed two-fold increased activity, with an IC_{50} value of 62 nM. Surprisingly, carboxamide-substituted compounds **13f** and **13g** showed large decrease of the antagonistic effect, suggesting that the property of stronger hydrogen bonding acceptor of amide nitrogen

through the carbonyl oxygen, than ester might be involved in the interaction with hP2X7R.[39]

However, the quinolinone derivatives showed low inhibitory effects against BzATP-induced IL-1β release in LPS/IFNc-differentiated human THP-1 cells (Supporting Information, Table S3). To overcome the functional defects and improve the antagonistic activity, we tried to attempt to change substituent position from N^1 to C^2.[40] The results for the activities of quinolines are shown in Tables 4 and 5. At first, the effects of substituents at the R_2 and R_3 positions were re-explored with the 2-chloro-quinoline skeleton by employing the similar moieties investigated for the quinolinone derivatives in Table 1 (Table 4). Unlike the activity profile of quinolinone derivatives, no substitutions at the R_1 position (**13a** *vs* **16d**) and the cycloalkyl acetyl group at R_2 position (**11f**, **h** and **11i** *vs* **16c**, **e** and **16d**, respectively) were favorable for the 2-chloro-quinoline compounds. Therefore, the mode of antagonistic activity is speculated to be different between the skeletons. Among the quinoline derivatives listed in Table 4, compound **16c**, which possesses an adamantyl acetamide group at the 5 position of 2-chloro-quinoline, displayed single digit nanomolar antagonistic activity (IC_{50} = 4 nM).

To explore the effects of substituents at R_4 of the quinoline skeleton, various substituted phenyl groups (**17a**−**k**) were introduced by Suzuki coupling reactions with compound **16c** (Table 5). The different mode of action of quinoline analogs was re-confirmed by a comparison of compounds **11i** and **12j** (IC_{50} value of 120 nM and no activity at 1 μM, respectively) vs compounds **17a** and **17b** (IC_{50} values of 447 and 18 nM, respectively). Interestingly, demethylated derivative **17c** had two-fold increased activity, with high positional preference at the para position of the phenyl group compared with **17d** and **17e**. Therefore, further substitutions were tried with polar moieties having hydrogen donors and acceptors, including halide, amine, nitro, acid, ester and alcohol at the 4-position of R_4 phenyl group, resulting in 3 ~ 123 nM of IC_{50} values. The activity profile of the series of compounds

was as follows: no substitution (**17a**) < 4-chloro (**17f**) < 4-nitro (**17g**) < 4-methoxy (**17b**) < 4-amine (**17h**), 4-hydroxy (**17c**), 4-carboxylic acid (**17i**), 4-methyl ester (**17j**) < 4-hydroxymethyl (**17k**). Among the quinoline derivatives, compounds **16c** and **17k** showed potent antagonistic effects, with IC_{50} values of 4 and 3 nM, respectively. In addition, a parallel MTT assay[41] of active quinoline derivatives to evaluate their cytotoxicity resulted in more than 90% survival at 10 μM of the compounds (Table S4 and Table S5).

2.2.2. Functional Inhibitory Activities of IL-1β Release and Subtype Selectivity Among the quinolone derivatives, **16c**, **16e**, **17a**−**c** and **17f**−**k** were further evaluated for their functional activity based on P2X7R-related signaling in immune cells. The inhibitory activity of the antagonists on the IL-1β release triggered by the activation of P2X7R was measured in differentiated THP-1 cells. The trends of inhibitory activities of quinoline-based analogues in the IL-1β ELISA assay displayed a similar profile to the P2X7R antagonism in the EtBr uptake assay. Thus, the potent P2X7R antagonists with single digit nanomolar IC_{50} values, **16c**, **17c** and **17h**−**k** showed IC_{50} values of 7, 6, 12−33 nM in the suppression of IL-1β release.

To investigate P2XR subtype selectivity, the selected potent P2X7R antagonists **16c** and **17b** shown in Table 5 were evaluated at other P2XR subtypes. The antagonistic effects of the compounds were measured by their inhibition of Ca^{2+} flux in 1321N1 astrocytoma cells stably expressing the human P2X1−4 receptors. All compounds showed weak or negligible antagonistic activities at P2X1, 2 and 4 receptors and **17b** displayed an IC_{50} value of 3.0 μM for P2X3R (Table 6), indicating that this class of P2X7R antagonists has a good subtype selectivity profile.

2.2.3. Effects of P2X7R Antagonist on TS15-88 cells The potent P2X7R antagonists were

assessed for their anti-cancer effects using *in-vitro* assays of TS15-88 glioblastoma cells. TS15-88 neurosphere cells were incubated with a 0 or 50 μM concentration of each of the seven potent antagonists for 24 h and 72 h to measure cell viability. In figure 2, an inhibitory effect on TS15-88 cell viability was observed within 24 h for all agents, except compounds **17b** and **17i**. After 72 h of treatment, the seven antagonists showed an inhibitory effect on TS15-88 cells and showed higher effects than 24 h of treatment, except for **17i**. The IC_{50} values of selected compounds AZD9056, **16c**, **17c**, and **17j** were measured as 8.92, 40.0, 25.6, and 35.6 μM, respectively. As shown in figures 3 and 4, inhibitory effects on neurosphere formation were also observed for the seven antagonists. Except for **17i**, the antagonists showed over 50 percent critical inhibitory effects on sphere formation after 5 days of 50 μM drug treatment. In mRNA expression studies of TS15-88 cells after drug treatment, genes that represent functions of maintaining stemness within the cells were changed. As shown in figure 5, POU5F1 expression was significantly reduced by 41% after 3 days of **16c** treatment. SOX2 expression did not show any changes. Interestingly, MYC and CD133 expression was increased by 41% and 30%, respectively, although the total surface area of the TS15-88 neurospheres was significantly decreased by 50 μM **16c** (Figures 3 and 4).

2.2.4. Blood-Brain Barrier (BBB) Permeability of P2X7R Antagonist on zebrafish models.

We have investigated *in vivo* BBB (blood-brain barrier) permeability of compound **16c** using the adult zebrafish models since targeting glioblastoma requires BBB penetration of drugs.[42] Zebrafish models have been applied for *in vivo* pharmacological studies because of its features such as small size, high fecundity and rapid growth. An adult male zebrafish was tested for the possibility of BBB penetration for the most active compound, **16c**. The concentration of **16c** at 0.5 h in the blood was measured as 235 ng/mL and 425 ng/mL in the

brain tissue, respectively (Figure 6 and Table 7), indicating that **16c** may have the property of significant BBB penetration.

2.2.5. Blood-Brain Barrier (BBB) Permeability test on Parallel Artificial Membrane Permeability Assay (PAMPA).

To investigate the BBB permeability of test compounds (**17c**, **17i**, **17k** and **17h**), we used PAMPA methods. The solubility at three concentrations before PAMPA proceeded at 50 μM, the highest concentration at which no precipitation of the compound occurs (Table 8-1).

2.2.6. Physicochemical Properties

As fundamental parameters of physicochemical properties, the water solubility and cell permeability of compound **16c**, **17c**, **17h** and **17k** showed medium level of kinetic solubility, and permeability (Table 9-2). The equilibrium solubility of **16c** resulted in more than 30 times less solubility than that of AZD9056. Unfortunately, the *in-vitro* metabolic stability of the compounds in liver microsomal fraction turned out to be very poor (Table 9-1). The lack of metabolic stability of some representative compounds needs to be improved for the optimization of oral bioavailability in the future.

3. Conclusions

Screening a quinolinone-based compound library led to the identification of **11a** as a new lead compound for P2X7R antagonism. To optimize P2X7R antagonistic potency, modifications at R_1, R_2 and R_3 of the quinolinone structure were performed. SAR analysis of the various derivatives suggested that a carboxylate ethyl ester group at R_1, adamantyl carboxamide at R_2 and 4-methoxy substitution at R_3 gave the best substituents for the antagonism of P2X7R activity. Since the quinolinones showed low functional inhibitory effects in an IL-1β ELISA assay, further modification of the core structure was examined. The resulting optimized quinoline-based antagonists, **16c** and **17k**, showed single digit nanomolar IC_{50} values in both EtBr uptake and IL-1β ELISA assays. Furthermore, the most potent representative antagonist, **16c**, displayed appreciable functional activities in reducing the sphere size of TS15-88 glioblastoma cells. These results suggest that the quinoline-based P2X7R antagonists may have the potential to treat glioblastoma, which is currently categorized as highly unmet medical needs.

4. Experimental section

4.1. Chemistry

All the reagents and solvents were purchased from Sigma-Aldrich and TCI and used without further purification. ^{1}H NMR spectra were determined with a JEOL JNM-ECX 400P spectrometer at 400 MHz, and ^{13}C NMR spectra were recorded using a FT-NMR spectrometer at 125 MHz (Korea Basic Science Institute, Gwangju); spectra were taken in $CDCl_3$, DMSO-d_6 or MeOH-d_4. Unless otherwise noted, chemical shifts are expressed as δ units downfield from internal tetramethylsilane or relative parts per million (ppm) from $CDCl_3$ (7.26 ppm), DMSO (2.50 ppm), MeOH (3.31 ppm) and coupling constants (*J*) are in Hertz (Hz). Data are reported as follows: chemical shift, multiplicity (s, singlet; d, doublet; t, triplet; m, multiplet), coupling constants and integration. Mass spectroscopy was carried out on electrospray, and high-resolution mass spectra (m/z) were recorded on FAB and ESI. High-resolution mass analysis was performed at Korea Basic Science Institute (Daegu) and National Development Institute of Korean Medicine (Jangheung-Gun).

The purity of all final compounds was determined by analytical HPLC. The determination of purity was conducted on Agilent 1100 series HPLC system using an Agilent ZORBAX Extend C18 analytical column (250 × 4.6 mm, 5 mm, 80 Å) in linear gradient solvent systems (solvent system was H_2O:CH_3CN = 80:20 over 10 min at a flow of 1 mL min^{-1}). Peaks were detected at 254 nm.

5-Nitroquinolin-2(1H)-one (9a) See reference 38.

Methyl 5-nitro-2-oxo-1,2-dihydroquinoline-3-carboxylate (9b) See reference 32.

General procedure A: For preparation of 10a–l, 15a–b and 17h

Appropriate benzyl substituted compounds,[37] **14a**–**b** or **17g** (1.0 equiv) was dissolved in ethanol and $SnCl_2$ (3.0 equiv) was added. After the reaction mixture was stirred for 4 h at 80 ^oC in argon gas environment, it was concentrated and partitioned between saturate brine and ethyl acetate. The organic layer was dried over sodium sulfate, filtered and evaporated under the vacuum. The resulting residue was purified by silica gel column chromatography to afford **10a**–**l**, **15a**–**b** and **17h**.

5-Amino-1-(4-methoxybenzyl)quinolin-2(1H)-one (10a) Following the general procedure **A**, reaction of **1-(4-methoxybenzyl)-5-nitroquinolin-2(1H)-one** (Supporting Information) (80.0 mg, 0.25 mmol) with $SnCl_2$ (169.0 mg, 0.75 mmol) in EtOH affords **10a** (62.0 mg). Yield 89%; ^{1}H NMR (400 MHz, $CDCl_3$) δ 7.61 (1H, d, *J* = 8.0 Hz), 7.31 (1H, t, *J* = 8.0 Hz), 7.03 (2H, d, *J* = 8.0 Hz), 6.83–6.81 (2H, m), 6.73 (2H, d, *J* = 8.0 Hz), 6.48 (1H, d, *J* = 8.0 Hz), 5.46 (2H, s), 4.11 (2H, s), 3.76 (3H, s). MS (ESI) *m/z*: 281.96 ($[M+H]^+$).

Methyl 5-amino-1-(4-methoxybenzyl)-2-oxo-1,2-dihydroquinoline-3-carboxylate (10b) See reference 32.

Methyl 5-amino-1-(3-methoxybenzyl)-2-oxo-1,2-dihydroquinoline-3-carboxylate (10c) Following the general procedure **A**, reaction of **methyl 1-(3-methoxybenzyl)-5-nitro-2-oxo-1,2-dihydroquinoline-3-carboxylate**[37] (80.0 mg, 0.21 mmol) with $SnCl_2$ (147.0 mg, 0.65

mmol) in EtOH affords **10c** (153.0 mg). Yield 70%; ^{1}H NMR (400 MHz, $CDCl_3$) δ 8.69 (1H, s), 7.81 (1H, dd, *J* = 4.0 Hz, 4.0 Hz), 7.62 (1H, t, *J* = 8.0 Hz), 7.53 (1H, d, *J* = 8.0 Hz), 7.22–7.16 (2H, m), 7.00 (2H, t, *J* = 8.0 Hz), 5.51 (2H, s), 4.38 (2H, s), 3.97 (3H, s), 3.75 (3H, s). MS (ESI) *m/z*: 338.87 ($[M+H]^+$).

Methyl 5-amino-2-oxo-1-(4-(trifluoromethoxy)benzyl)-1,2-dihydroquinoline-3-carboxylate (10d) Following the general procedure **A**, reaction of **methyl 5-nitro-2-oxo-1-(4-(trifluoromethoxy)benzyl)-1,2-dihydroquinoline-3-carboxylate**[37] (80.0 mg, 0.18 mmol) with $SnCl_2$ (128.0 mg, 0.56 mmol) in EtOH affords **10d** (72.0 mg). Yield 100%; ^{1}H NMR (400 MHz, $CDCl_3$) δ 8.70 (1H, s), 7.62 (1H, d, *J* = 8.0 Hz), 7.36–7.27 (4H, m), 6.53–6.46 (2H, m), 5.50 (2H, s), 4.45 (2H, s), 3.98 (3H, s). MS (ESI) *m/z*: 391.10 ($[M-H]^-$).

Methyl 5-amino-1-(4-fluorobenzyl)-2-oxo-1,2-dihydroquinoline-3-carboxylate (10e) Following the general procedure **A**, reaction of **methyl 1-(4-fluorobenzyl)-5-nitro-2-oxo-1,2-dihydroquinoline-3-carboxylate**[37] (80.0 mg, 0.22 mmol) with $SnCl_2$ (152.0 mg, 0.67 mmol) in EtOH affords **10e** (199.0 mg). Yield 91%; ^{1}H NMR (400 MHz, $CDCl_3$) δ 8.70 (1H, s), 7.60 (1H, t, *J* = 8.0 Hz), 7.51 (1H, d, *J* = 8.0 Hz), 7.42 (1H, d, *J* = 8.0 Hz), 7.10 (2H, dd, *J* = 4.0 Hz, 8.0 Hz), 6.97 (2H, t, *J* = 8.0 Hz), 5.50 (2H, s), 4.43 (2H, s), 3.91 (3H, s). MS (ESI) *m/z*: 325.23 ($[M-H]^-$).

Methyl 5-amino-1-(4-chlorobenzyl)-2-oxo-1,2-dihydroquinoline-3-carboxylate (10f) Following the general procedure **A**, reaction of **methyl 1-(4-chlorobenzyl)-5-nitro-2-oxo-1,2-dihydroquinoline-3-carboxylate**[37] (80.0 mg, 0.21 mmol) with $SnCl_2$ (145.0 mg, 0.64 mmol) in EtOH affords **10f** (55.0 mg). Yield 76%; ^{1}H NMR (400 MHz, $CDCl_3$) δ 8.74 (1H,

s), 7.66 (1H, d, *J* = 8.0 Hz), 7.63 (1H, t, *J* = 8.0 Hz), 7.50 (1H, d, *J* = 8.0 Hz), 7.30 (2H, d, *J* = 8.0 Hz), 7.17 (2H, d, *J* = 8.0 Hz), 5.52 (2H, s), 4.40 (2H, s), 3.91(3H, s). MS (ESI) *m/z*: 341.23 ($[M-H]^-$).

Methyl 5-amino-1-(4-bromobenzyl)-2-oxo-1,2-dihydroquinoline-3-carboxylate (10g) Following the general procedure **A**, reaction of **methyl 1-(4-bromobenzyl)-5-nitro-2-oxo-1,2-dihydroquinoline-3-carboxylate**[37] (80.0 mg, 0.19 mmol) with $SnCl_2$ (130.0 mg, 0.57 mmol) in EtOH affords **10g** (57.0 mg). Yield 77%; ^{1}H NMR (400 MHz, $CDCl_3$) δ 8.63 (1H, s), 7.84–7.81 (1H, m), 7.60 (1H, t, *J* = 8.0 Hz), 7.48–7.41 (3H, m), 7.10 (2H, d, *J* = 8.0 Hz), 5.50 (2H, s), 4.43 (2H, s), 3.84 (3H, s). MS (ESI) *m/z*: 387.73 ($[M+H]^+$).

Methyl 5-amino-1-(4-methylbenzyl)-2-oxo-1,2-dihydroquinoline-3-carboxylate (10h) Following the general procedure **A**, reaction of **methyl 1-(4-methylbenzyl)-5-nitro-2-oxo-1,2-dihydroquinoline-3-carboxylate**[37] (80.0 mg, 0.22 mmol) with $SnCl_2$ (153.0 mg, 0.68 mmol) in EtOH affords **10h** (71.0 mg). Yield 100%; ^{1}H NMR (400 MHz, $CDCl_3$) δ 8.62 (1H, s), 7.73–7.70 (1H, m), 7.58–7.48 (2H, m), 7.20–7.00 (4H, m), 5.50 (2H, s), 4.40 (2H, s), 3.94 (3H, s), 2.31 (3H, s). MS (ESI) *m/z*: 321.03 ($[M-H]^-$).

Methyl 5-amino-1-(4-ethylbenzyl)-2-oxo-1,2-dihydroquinoline-3-carboxylate (10i) Following the general procedure **A**, reaction of **methyl 1-(4-ethylbenzyl)-5-nitro-2-oxo-1,2-dihydroquinoline-3-carboxylate**[37] (80.0 mg, 0.21 mmol) with $SnCl_2$ (147.0 mg, 0.65 mmol) in EtOH affords **10i** (63.0 mg). Yield 89%; ^{1}H NMR (400 MHz, $CDCl_3$) δ 8.68 (1H, s), 7.80–7.70 (1H, m), 7.53–7.46 (2H, m), 7.10–7.00 (4H, m), 5.49 (2H, s), 4.37 (2H, s), 3.97 (3H, s), 2.62–2.49 (2H, m), 1.20 (3H, t, *J* = 8.0 Hz). MS (ESI) *m/z*: 336.92 ($[M+H]^+$).

Methyl 5-amino-1-(4-nitrobenzyl)-2-oxo-1,2-dihydroquinoline-3-carboxylate (10j) Following the general procedure **A**, reaction of **methyl 5-nitro-1-(4-nitrobenzyl)-2-oxo-1,2-dihydroquinoline-3-carboxylate**[37] (80.0 mg, 0.20 mmol) with $SnCl_2$ (137.0 mg, 0.61 mmol) in EtOH affords **10j** (68.0 mg). Yield 96%; ^{1}H NMR (400 MHz, $CDCl_3$) δ 8.70 (1H, d, *J* = 8.0 Hz), 8.15 (2H, d, *J* = 12.0 Hz), 7.41–7.32 (2H, m), 7.31–7.27 (1H, m), 6.51 (1H, d, *J* = 8.0 Hz), 6.49–6.41 (1H, m), 5.59 (2H, s), 4.45 (2H, s), 3.98 (3H, s). MS (ESI) *m/z*: 351.76 ($[M-H]^-$).

Methyl 5-amino-1-(4-cyanobenzyl)-2-oxo-1,2-dihydroquinoline-3-carboxylate (10k) Following the general procedure **A**, reaction of **methyl 1-(4-cyanobenzyl)-5-nitro-2-oxo-1,2-dihydroquinoline-3-carboxylate**[37] (80.0 mg, 0.21 mmol) with $SnCl_2$ (149.0 mg, 0.66 mmol) in EtOH affords **10k** (58.0 mg). Yield 78%; ^{1}H NMR (400 MHz, $CDCl_3$) δ 8.74 (1H, s), 7.60 (1H, d, *J* = 8.0 Hz), 7.33–7.27 (4H, m), 6.53–6.46 (2H, m), 5.56 (2H, s), 4.45 (2H, s), 3.98 (3H, s). MS (ESI) *m/z*: 334.84 ($[M+H]^+$).

Methyl 5-amino-1-benzyl-2-oxo-1,2-dihydroquinoline-3-carboxylate (10l) Following the general procedure **A**, reaction of **methyl 1-benzyl-5-nitro-2-oxo-1,2-dihydroquinoline-3-carboxylate**[37] (80.0 mg, 0.23 mmol) with $SnCl_2$ (155.0 mg, 0.69 mmol) in EtOH affords **10l** (62.0 mg). Yield 87%; ^{1}H NMR (400 MHz, $CDCl_3$) 8.79 (1H, s), 7.61 (1H, d, *J* = 8.0 Hz), 7.34–7.32 (2H, m), 7.22 (3H, t, *J* = 8.0 Hz), 6.54 (2H, d, *J* = 8.0 Hz), 5.52 (2H, s), 4.43 (2H, s), 3.99 (3H, s). MS (ESI) *m/z*: 309.10 ($[M+H]^+$).

2-Chloroquinolin-5-amine (15a) Following the general procedure **A**, reaction of **14a** (75.0 mg, 0.36 mmol) with $SnCl_2$ (243.0 mg, 1.08 mmol) in EtOH affords **15a** (72.0 mg). Yield 100%; ^{1}H NMR (400 MHz, $CDCl_3$) δ 8.07 (1H, d, *J* = 8.0 Hz), 7.48 (1H, t, *J* = 8.0 Hz), 7.42 (1H, d, *J* = 8.0 Hz), 7.27 (1H, d, *J* = 8.0 Hz), 6.78 (1H, dd, *J* = 8.0 Hz, 8.0 Hz). MS (ESI) *m/z*: 177.54 ($[M-H]^-$).

Methyl 5-amino-2-chloroquinoline-3-carboxylate (15b) Following the general procedure **A**, reaction of **14b** (80.0 mg, 0.30 mmol) with $SnCl_2$ (1.0 mg, 0.90 mmol) in EtOH affords **15b** (72.0 mg). Yield 100 %; ^{1}H NMR (400 MHz, $CDCl_3$) δ 8.75 (1H, s), 7.61 (1H, t, *J* = 8.0 Hz), 7.45 (1H, d, *J* = 8.0 Hz), 6.83 (1H, dd, *J* = 8.0 Hz, 8.0 Hz), 3.99 (3H, s). MS (ESI) *m/z*: 237.30 ($[M+H]^+$).

2-(Adamantan-1-yl)-N-(2-(4-aminophenyl)quinolin-5-yl)acetamide (17h) Following the general procedure **A**, reaction of **17g** (10.0 mg, 0.02 mmol) with $SnCl_2$ (15.0 mg, 0.06 mmol) in EtOH affords **17h** (3.0 mg). Yield 30%; ^{1}H NMR (400 MHz, $CDCl_3$) δ 8.15 (1H, d, *J* = 8.0 Hz), 8.01 (2H, d, *J* = 8.0 Hz), 7.95 (1H, d, *J* = 8.0 Hz), 7.81 (1H, d, *J* = 8.0 Hz), 7.49–7.40 (2H, m), 7.34 (1H, s), 6.79 (2H, d, *J* = 8.0 Hz), 3.87 (2H, s), 2.26 (2H, s), 2.18 (1H, s), 2.04 (1H, s), 1.79–1.63 (13H, m). MS (ESI) *m/z*: 412.19 ($[M+H]^+$). Purity 96%

General procedure B: For preparation of 11a–i, 12a–j, 13a and 16a–e

Compounds **10a**–**l**, **15a** or **15b** (1.0 equiv), DIPEA (2.0 equiv) and appropriate carboxylic acid chloride derivative (1.2 equiv) were stirred in DCM for 15 min at room temperature.

After the reaction mixture was partitioned between saturated aqueous $NaHCO_3$ solution and ethyl acetate. The organic layer was dried over sodium sulfate, filtered and evaporated under vacuum. The resulting residue was purified by silica gel column chromatography to afford **11a**–**i**, **12a**–**j**, **13a** and **16a**–**e**.

Methyl 1-(4-methoxybenzyl)-2-oxo-5-(3-phenylpropanamido)-1,2-dihydroquinoline-3-carboxylate (11a) Following the general procedure **B**, acylation reaction of **10b** (10.0 mg, 0.02 mmol) and hydrocinnamoyl chloride (0.005 mL, 0.03 mmol) affords **11a** (4.9 mg). Yield 35%; ^{1}H NMR (400 MHz, $CDCl_3$) δ 8.22 (1H, s), 7.56 (1H, s), 7.36 (1H, t, *J* = 8.0 Hz), 7.21–7.15 (5H, m), 6.90 (1H, d, *J* = 8.0 Hz), 6.84–6.77 (4H, m), 6.58 (1H, d, *J* = 8.0 Hz), 5.48 (2H, s), 3.96 (3H, s), 3.75 (3H, s), 3.18–3.01 (4H, m). MS (ESI) *m/z*: 471.13 ($[M+H]^+$). Purity 96%.

Methyl 1-(4-methoxybenzyl)-2-oxo-5-(2-phenylacetamido)-1,2-dihydroquinoline-3-carboxylate (11b) Following the general procedure **B**, acylation reaction of **10b** (10.0 mg, 0.02 mmol) and phenylacetyl chloride (0.004 mL, 0.03 mmol) affords **11b** (4.0 mg). Yield 30%; ^{1}H NMR (400 MHz, $CDCl_3$) δ 8.19 (1H, s), 7.57–7.36 (6H, m), 7.32–7.27 (2H, m), 7.24–7.20 (1H, m), 7.12 (2H, d, *J* = 8.0 Hz), 6.78 (2H, d, *J* = 8.0 Hz), 5.45 (2H, s), 3.95 (3H, s), 3.76 (3H, s), 2.16–2.14 (2H, m). MS (ESI) *m/z*: 455.39 ($[M-H]^-$). Purity 99%

Methyl 5-benzamido-1-(4-methoxybenzyl)-2-oxo-1,2-dihydroquinoline-3-carboxylate (11c) Following the general procedure **B**, acylation reaction of **10b** (10.0 mg, 0.02 mmol) and

benzoyl chloride (0.004 mL, 0.03 mmol) affords **11c** (5.0 mg). Yield 39%; ^{1}H NMR (400 MHz, $CDCl_3$) δ 8.62 (1H, s), 8.24 (1H, s), 7.97 (2H, d, *J* = 8.0 Hz), 7.64–7.58 (2H, m), 7.57–7.49 (3H, m), 7.24–7.20 (1H, m), 7.16 (2H, d, *J* = 8.0 Hz), 6.82 (2H, d, *J* = 8.0 Hz), 5.46 (2H, s), 3.91 (3H, s), 3.73 (3H, s). MS (ESI) *m/z*: 441.39 ($[M-H]^-$). Purity 96%

Methyl 5-(3-cyclopentylpropanamido)-1-(4-methoxybenzyl)-2-oxo-1,2-dihydroquinoline-3-carboxylate (11d) Following the general procedure **B**, acylation reaction of **10b** (10.0 mg, 0.02 mmol) and cyclopentanepropionyl chloride (0.004 mL, 0.03 mmol) affords **11d** (5.0 mg). Yield 37%; ^{1}H NMR (400 MHz, MeOH-d_4) 8.25 (1H, s), 7.78 (1H, s), 7.47 (1H, t, *J* = 8.0 Hz), 7.15 (2H, d, *J* = 8.0 Hz), 7.04 (1H, d, *J* = 8.0 Hz), 6.84 (1H, d, *J* = 8.0 Hz), 6.78 (2H, d, *J* = 8.0 Hz), 5.53 (2H, s), 3.93 (3H, s), 3.74 (3H, s), 3.18–3.01 (4H, m), 2.23–2.18 (9H, m). MS (ESI) *m/z*: 463.12 ($[M+H]^+$). Purity 95%

Methyl 5-(3-cyclohexylpropanamido)-1-(4-methoxybenzyl)-2-oxo-1,2-dihydroquinoline-3-carboxylate (11e) Following the general procedure **B**, acylation reaction of **10b** (10.0 mg, 0.02 mmol) and 3-cyclohexylpropanoyl chloride (6.0 mg, 0.03 mmol) affords **11e** (5.0 mg). Yield 36%; ^{1}H NMR (400 MHz, $CDCl_3$) δ 8.62 (1H, s), 7.70 (1H, s), 7.52–7.48 (2H, m), 7.15 (3H, d, *J* = 8.0 Hz), 6.81 (2H, d, *J* = 8.0 Hz), 5.49 (2H, s), 4.46–4.41 (2H, m), 3.75 (3H, s), 2.52 (2H, m), 2.33–2.29 (7H, m), 1.54–1.50 (7H, m). MS (ESI) *m/z*: 476.79 ($[M+H]^+$). Purity 95%

Methyl 5-(2-cyclohexylacetamido)-1-(4-methoxybenzyl)-2-oxo-1,2-dihydroquinoline-3-carboxylate (11f) Following the general procedure **B**, acylation reaction of **10b** (10.0 mg, 0.02 mmol) and cyclohexylacetyl chloride (0.004 mL, 0.03 mmol) affords **11f** (5.0 mg). Yield 37%; ^{1}H NMR (400 MHz, $CDCl_3$) δ 8.62 (1H, s), 7.55–7.49 (2H, m), 7.40 (1H, s), 7.17 (3H, d, *J* = 8.0 Hz), 6.82 (2H, d, *J* = 8.0 Hz), 5.52 (2H, s), 3.97 (3H, s), 3.76 (3H, s), 2.40–2.30 (2H, m), 2.08–1.98 (3H, m), 1.91–1.84 (3H, m), 1.76–1.69 (2H, m), 1.65–1.60 (3H, m). MS (ESI) *m/z*: 461.48 ($[M-H]^-$). Purity 95%

Methyl 5-(cyclohexanecarboxamido)-1-(4-methoxybenzyl)-2-oxo-1,2-dihydroquinoline-3-carboxylate (11g) Following the general procedure **B**, acylation reaction of **10b** (5.0 mg, 0.01 mmol) and cyclohexanecarbonyl chloride (0.002 mL, 0.02 mmol) affords **11g** (1.0 mg). Yield 17%; ^{1}H NMR (400 MHz, $CDCl_3$) δ 8.57 (1H, s), 7.51 (2H, d, *J* = 8.0 Hz), 7.38 (1H, s), 7.16 (3H, d, *J* = 8.0 Hz), 6.81 (2H, d, *J* = 8.0 Hz), 5.49 (2H, s), 3.98 (3H, s), 3.74 (3H, s), 2.08–1.98 (3H, m), 1.91–1.84 (3H, m), 1.76–1.69 (2H, m), 1.65–1.60 (3H, m). MS (ESI) *m/z*: 448.91 ($[M+H]^+$). Purity 99%

Methyl 5-(2-(adamantan-1-yl)acetamido)-1-(4-methoxybenzyl)-2-oxo-1,2-dihydroquinoline-3-carboxylate (11h) Following the general procedure **B**, acylation reaction of **10b** (10.0 mg, 0.02 mmol) and 1-adamantane acetyl chloride (0.006 mL, 0.03 mmol) affords **11h** (5.0 mg). Yield 33%; ^{1}H NMR (400 MHz, $CDCl_3$) δ 8.64 (1H, s), 7.52–7.49 (2H, m), 7.35 (1H, s), 7.16 (3H, d, *J* = 8.0 Hz), 6.82 (2H, d, *J* = 8.0 H), 5.52 (2H, s), 3.96 (3H, s), 3.76 (3H, s), 2.23–2.20 (2H, m), 2.16 (1H, s), 2.02 (1H, s), 1.79–1.63 (13H, m). MS (ESI) *m/z*: 513.45 ($[M-H]^-$). Purity 95%

Methyl 5-(adamantane-1-carboxamido)-1-(4-methoxybenzyl)-2-oxo-1,2-dihydroquinoline-3-carboxylate (11i) Following the general procedure **B**, acylation reaction of **10b** (10.0 mg, 0.02 mmol) and adamantane-1-carbonyl chloride (6.0 mg, 0.03 mmol) affords **11i** (4.0 mg). Yield 27%; ^{1}H NMR (400 MHz, $CDCl_3$) δ 8.55 (1H, s), 7.58 (1H, s), 7.51 (1H, t, *J* = 8.0 H), 7.45 (1H, d, *J* = 8.0 Hz), 7.16 (3H, t, *J* = 8.0 Hz), 6.81 (2H, d, *J* = 8.0 Hz), 5.47 (2H, s), 3.98 (3H, s), 3.76 (3H, s), 2.18 (1H, s), 2.04 (1H, s), 1.79–1.63 (13H, m). ^{13}C NMR (125 MHz, $CDCl_3$) 206.86, 176.98, 165.88, 158.79, 158.62, 141.97, 138.81, 135.82, 133.34, 128.08, 127.90, 127.87, 121.51, 119.03, 114.22, 113.84, 112.84, 55.24, 52.88, 46.19, 41.80, 39.35, 38.65, 36.31, 30.93, 28.11, 27.81. MS (ESI) *m/z*: 501.47 ($[M+H]^+$). HRMS (FAB) calcd for $C_{30}H_{32}N_2O_5$ $[M]^+$ 500.2311, found 500.2310. Purity 97%

Methyl 5-(adamantane-2-carboxamido)-1-(3-methoxybenzyl)-2-oxo-1,2-dihydroquinoline-3-carboxylate (12a) Following the general procedure **B**, acylation reaction of **10c** (10.0 mg, 0.02 mmol) and adamantane-1-carbonyl chloride (6.0 mg, 0.03 mmol) affords **12a** (4.0 mg). Yield 27%; ^{1}H NMR (400 MHz, $CDCl_3$) δ 8.57 (1H, s), 7.58 (1H, s), 7.53–7.43 (2H, m), 7.20 (1H, t, *J* = 8.0 Hz), 7.13 (1H, d, *J* = 8.0 Hz), 6.77–6.74 (3H, m), 5.55 (2H, s), 3.99 (3H, s), 3.75 (3H, s), 2.18 (1H, s), 2.04 (1H, s), 1.79–1.63 (13H, m). MS (ESI) *m/z*: 500.94 ($[M+H]^+$). Purity 97%

Methyl 5-(adamantane-2-carboxamido)-2-oxo-1-(4-(trifluoromethoxy)benzyl)-1,2-dihydroquinoline-3-carboxylate (12b) Following the general procedure **B**, acylation

reaction of **10d** (10.0 mg, 0.02 mmol) and adamantane-1-carbonyl chloride (6.0 mg, 0.03 mmol) affords **12b** (4.0 mg). Yield 28%; ^{1}H NMR (400 MHz, $CDCl_3$) δ 8.68 (1H, s), 7.57–7.51 (2H, m), 7.42 (1H, s), 7.24–7.19 (2H, m), 7.14 (2H, d, *J* = 8.0 Hz), 7.10–7.07 (1H, m), 5.54 (2H, s), 3.95 (3H, s), 2.18 (1H, s), 2.04 (1H, s), 1.79–1.63 (13H, m). MS (ESI) *m/z*: 553.51 ($[M-H]^-$). Purity 97%

Methyl 5-(adamantane-2-carboxamido)-1-(4-fluorobenzyl)-2-oxo-1,2-dihydroquinoline-3-carboxylate (12c) Following the general procedure **B**, acylation reaction of **10e** (10.0 mg, 0.03 mmol) and adamantane-1-carbonyl chloride (6.0 mg, 0.03 mmol) affords **12c** (5.0 mg). Yield 34%; ^{1}H NMR (400 MHz, $CDCl_3$) δ 8.53 (1H, s), 7.55 (1H, s), 7.53–7.46 (2H, m), 7.44 (1H, t, *J* = 8.0 Hz), 7.21–7.17 (2H, m), 6.97 (2H, t, *J* = 8.0 Hz), 5.52 (2H, s), 3.98 (3H, s), 2.18 (1H, s), 2.04 (1H, s), 1.79–1.63 (13H, m). MS (ESI) *m/z*: 488.92 ($[M+H]^+$). Purity 95%

Methyl 5-(adamantane-2-carboxamido)-1-(4-chlorobenzyl)-2-oxo-1,2-dihydroquinoline-3-carboxylate (12d) Following the general procedure **B**, acylation reaction of **10f** (10.0 mg, 0.02 mmol) and adamantane-1-carbonyl chloride (6.0 mg, 0.03 mmol) affords **12d** (5.0 mg). Yield 34%; ^{1}H NMR (400 MHz, $CDCl_3$) δ 8.53 (1H, s), 7.55 (1H, s), 7.53–7.28 (3H, m), 7.14–7.00 (3H, m), 6.97 (1H, t, *J* = 8.0 Hz), 5.53 (2H, s), 3.91 (3H, s), 2.18 (1H, s), 2.04 (1H, s), 1.79–1.63 (13H, m). MS (ESI) *m/z*: 505.92 ($[M+H]^+$). Purity 96%

Methyl 5-(adamantane-2-carboxamido)-1-(4-bromobenzyl)-2-oxo-1,2-dihydroquinoline-3-carboxylate (12e) Following the general procedure **B**, acylation reaction of **10g** (10.0 mg,

0.02 mmol) and adamantane-1-carbonyl chloride (6.0 mg, 0.03 mmol) affords **12e** (5.0 mg). Yield 36%; ^{1}H NMR (400 MHz, $CDCl_3$) δ 8.51 (1H, s), 7.55 (1H, s), 7.53–7.41 (2H, m), 7.31–7.28 (2H, m), 7.11–7.00 (2H, m), 6.97–6.94 (1H, m), 5.52 (2H, s), 3.98 (3H, s), 2.18 (1H, s), 2.04 (1H, s), 1.79–1.63 (13H, m). MS (ESI) *m/z*: 549.12 ($[M+H]^+$). Purity 96%

Methyl 5-(adamantane-2-carboxamido)-1-(4-methylbenzyl)-2-oxo-1,2-dihydroquinoline-3-carboxylate (12f) Following the general procedure **B**, acylation reaction of **10h** (10.0 mg, 0.03 mmol) and adamantane-1-carbonyl chloride (7.0 mg, 0.03 mmol) affords **12f** (5.0 mg). Yield 34%; ^{1}H NMR (400 MHz, $CDCl_3$) δ 8.56 (1H, s), 7.55 (1H, s), 7.53–7.43 (3H, m), 7.23–7.09 (3H, m), 6.97 (1H, t, *J* = 8.0 Hz), 5.52 (2H, s), 3.95 (3H, s), 2.42 (3H, s), 2.18 (1H, s), 2.04 (1H, s), 1.79–1.63 (13H, m). MS (ESI) *m/z*: 483.92 ($[M-H]^-$). Purity 99%

Methyl 5-(adamantane-2-carboxamido)-1-(4-ethylbenzyl)-2-oxo-1,2-dihydroquinoline-3-carboxylate (12g) Following the general procedure **B**, acylation reaction of **10i** (10.0 mg, 0.02 mmol) and adamantane-1-carbonyl chloride (6.0 mg, 0.03 mmol) affords **12g** (4.0 mg). Yield 27%; ^{1}H NMR (400 MHz, DMSO-d_6) 8.56 (1H, s), 7.55 (1H, s), 7.51 (1H, t, *J* = 8.0 Hz), 7.28 (1H, d, *J* = 8.0 Hz), 7.13–7.06 (5H, m), 5.47 (2H, s), 3.80 (3H, s), 2.52–2.49 (2H, m), 2.03–1.84 (9H, m), 1.74–1.63 (9H, m). MS (ESI) *m/z*: 498.93 ($[M+H]^+$). Purity 96%

Methyl 5-(adamantane-2-carboxamido)-1-(4-nitrobenzyl)-2-oxo-1,2-dihydroquinoline-3-carboxylate (12h) Following the general procedure **B**, acylation reaction of **10j** (10.0 mg, 0.02 mmol) and adamantane-1-carbonyl chloride (6.0 mg, 0.03 mmol) affords **12h** (4.0 mg).

Yield 27%; ^{1}H NMR (400 MHz, $CDCl_3$) δ 8.60 (1H, s), 8.16 (2H, d, *J* = 8.0 Hz), 7.60 (1H, s), 7.54–7.46 (2H, m), 7.36 (2H, d, *J* = 8.0 Hz), 7.00–6.96 (1H, m), 5.65 (2H, s), 3.98 (3H, s), 2.18 (1H, s), 2.04 (1H, s), 1.79–1.63 (13H, m). MS (ESI) *m/z*: 513.84 ($[M-H]^-$). Purity 95%

Methyl 5-(adamantane-1-carboxamido)-1-(4-cyanobenzyl)-2-oxo-1,2-dihydroquinoline-3-carboxylate (12i) Following the general procedure **B**, acylation reaction of **10k** (10.0 mg, 0.03 mmol) and adamantane-1-carbonyl chloride (7.0 mg, 0.03 mmol) affords **12i** (4.0 mg). Yield 26%; ^{1}H NMR (400 MHz, $CDCl_3$) δ 8.59 (1H, s), 7.59 (2H, d, *J* = 8.0 Hz), 7.55–7.43 (2H, m), 7.30 (2H, d, *J* = 8.0 Hz), 7.00 (1H, d, *J* = 8.0 Hz), 5.62 (2H, s), 3.99 (3H, s), 2.18 (1H, s), 2.04 (1H, s), 1.79–1.63 (13H, m). MS (ESI) *m/z*: 495.90 ($[M+H]^+$). Purity 95%

Methyl 5-(adamantane-1-carboxamido)-1-benzyl-2-oxo-1,2-dihydroquinoline-3-carboxylate (12j) Following the general procedure **B**, acylation reaction of **10l** (10.0 mg, 0.03 mmol) and adamantane-1-carbonyl chloride (7.0 mg, 0.03 mmol) affords **12j** (3.0 mg). Yield 22%; ^{1}H NMR (400 MHz, $CDCl_3$) δ 8.57 (1H, s), 7.60 (2H, d, *J* = 8.0 Hz), 7.55–7.43 (2H, m), 7.30–7.03 (4H, m), 5.60 (2H, s), 3.97 (3H, s), 2.18 (1H, s), 2.00 (1H, s), 1.79–1.60 (13H, m). MS (ESI) *m/z*: 469.21 ($[M-H]^-$). Purity 97%

N-(1-(4-Methoxybenzyl)-2-oxo-1,2-dihydroquinolin-5-yl)adamantane-2-carboxamide (13a) Following the general procedure **B**, acylation reaction of **10a** (10.0 mg, 0.03 mmol) and adamantane-1-carbonyl chloride (8.0 mg, 0.04 mmol) affords **13a** (7.0 mg). Yield 45%; ^{1}H NMR (400 MHz, $CDCl_3$) δ 7.73 (1H, d, *J* = 8.0 Hz), 7.47 (1H, s), 7.42–7.36 (2H, m), 7.20–

7.09 (3H, m), 6.86–6.74 (3H, m), 5.50 (2H, s), 3.76 (3H, s), 2.18 (1H, s), 2.04 (1H, s), 1.79–1.63 (13H, m). MS (ESI) *m/z*: 442.91 ($[M+H]^+$). Purity 99%

Methyl 5-(2-(adamantan-1-yl)acetamido)-2-chloroquinoline-3-carboxylate (16a) Following the general procedure **B**, acylation of **15b** (5.0 mg, 0.02 mmol) and 1-adamantaneacetylchloride (0.003 mL, 0.02 mmol) in DCM affords **16a** (4.0 mg). Yield 48%; ^{1}H NMR (400 MHz, $CDCl_3$) δ 8.62 (1H, s), 7.93–7.77 (3H, m), 7.67 (1H, s), 4.01 (3H, s), 2.30 (2H, s), 2.18 (1H, s), 2.04 (1H, s), 1.79–1.63 (13H, m). MS (ESI) *m/z*: 413.52 ($[M+H]^+$). Purity 94%

Methyl 5-(adamantane-1-carboxamido)-2-chloroquinoline-3-carboxylate (16b) Following the general procedure **B**, acylation of **15b** (5.0 mg, 0.02 mmol) and adamantane-1-carbonyl chloride (3.0 mg, 0.02 mmol) in DCM affords **16b** (4.0 mg). Yield 48%; ^{1}H NMR (400 MHz, $CDCl_3$) δ 8.62 (1H, s), 7.93–7.73 (3H, m), 7.65 (1H, s), 4.04 (3H, s), 2.18 (1H, s), 2.04 (1H, s), 1.79–1.63 (13H, m). MS (ESI) *m/z*: 399.01 ($[M+H]^+$). Purity 97%

2-(Adamantan-1-yl)-N-(2-chloroquinolin-5-yl)acetamide (16c) Following the general procedure **B**, acylation of **15a** (50.0 mg, 0.28 mmol) and 1-adamantaneacetylchloride (0.06 mL, 0.33 mmol) in DCM affords **16c** (37.0 mg). Yield 37%; ^{1}H NMR (400 MHz, $CDCl_3$) δ 8.14 (1H, d, *J* = 8.0 Hz), 7.91 (1H, d, *J* = 8.0 Hz), 7.83 (1H, d, *J* = 8.0 Hz), 7.73 (1H, t, *J* = 8.0 Hz), 7.43 (1H, d, *J* = 8.0 Hz), 7.28 (1H, s), 2.24 (2H, s), 2.02 (2H, s), 1.79–1.63 (13H, m). ^{13}C NMR (125 MHz, $CDCl_3$) δ 144.35, 129.42, 128.21, 126.61, 122.68, 118.47, 118.28,

117.84, 110.00, 48.48, 38.83, 32.72, 30.59, 29.48, 26.94, 25.76, 24.65. MS (ESI) *m/z*: 352.98 ($[M-H]^-$). HRMS (ESI): calcd for $C_{21}H_{23}ClN_2O$ $[M+H]^+$ 355.1572, found. 355.2721. Purity 95%

N-(2-Chloroquinolin-5-yl)adamantane-1-carboxamide (16d) Following the general procedure **B**, acylation of **15a** (5.0 mg, 0.02 mmol) and 1-adamantane carbonyl chloride (4.0 mg, 0.02 mmol) in DCM affords **16d** (3.0 mg). Yield 44%; ^{1}H NMR (400 MHz, $CDCl_3$) δ 8.14 (1H, d, *J* = 8.0 Hz), 7.89 (1H, d, *J* = 8.0 Hz), 7.77 (1H, d, *J* = 8.0 Hz), 7.71 (1H, t, *J* = 8.0 Hz), 7.60 (1H, s), 7.39 (1H, d, *J* = 8.0 Hz), 2.18 (1H, s), 2.04 (1H, s), 1.79–1.63 (13H, m). MS (ESI) *m/z*: 340.90 ($[M+H]^+$). Purity 96%

N-(2-Chloroquinolin-5-yl)-2-cyclohexylacetamide (16e) Following the general procedure **B**, acylation of **15a** (5.0 mg, 0.02 mmol) and cyclohexylacetyl chloride (0.003 mL, 0.02 mmol) in DCM affords **16e** (2.0 mg). Yield 33%; ^{1}H NMR (400 MHz, $CDCl_3$) δ 8.12 (1H, d, *J* = 8.0 Hz), 7.87 (1H, d, *J* = 8.0 Hz), 7.75 (1H, d, *J* = 8.0 Hz), 7.71 (1H, t, *J* = 8.0 Hz), 7.66 (1H, s), 7.39 (1H, d, *J* = 8.0 Hz), 4.02–3.99 (2H, m), 3.02–2.13 (11H, m). ^{13}C NMR (125 MHz, $CDCl_3$) δ 146.97, 144.39, 129.34, 128.78, 126.58, 122.95, 118.62, 118.31, 117.93, 41.47, 31.67, 29.26, 27.01, 22.09. MS (ESI) *m/z*: 303.61 ($[M+H]^+$). Purity 98%

General procedure C: For preparation of 5-(adamantane-2-carboxamido)-1-(4-methoxybenzyl)-2-oxo-1,2-dihydroquinoline-3-carboxylic acid (13b) To a solution of 10% KOH in MeOH was added compounds **11i** (38.0 mg, 0.07 mmol). The reaction mixture was

stirred at 80 ^{o}C for 5 h. After being cooled, the reaction mixture was acidified with 1N HCl aqueous solution. Generated solid was dried washed with water to afford **13b** (35.0 mg). Yield 100%; ^{1}H NMR (400 MHz, $CDCl_3$) δ 14.48 (1H, s), 7.83 (1H, s), 7.74 (1H, d, *J* = 8.0 Hz), 7.67 (1H, t, *J* = 8.0 Hz), 7.32 (1H, d, *J* = 8.0 Hz), 7.15 (2H, d, *J* = 8.0 Hz), 6.87–6.84 (2H, m), 5.59 (2H, s), 3.77 (3H, s), 2.16 (3H, s), 2.08–2.07 (6H, m), 1.82–1.78 (6H, m). MS (ESI) *m/z*: 487.02 ($[M+H]^+$). Purity 96%

General procedure D: For preparation of 13c–e

A solution containing **13b** (1.0 equiv) in DCM was treated sequentially with appropriate alcohol derivative (1.0 equiv), EDC (3.0 equiv) and DMAP (0.1 equiv). After the reaction mixture was stirred at room temperature for 12 h, it was concentrated and partitioned between water and ethyl acetate. The organic layer was dried over sodium sulfate, filtered and evaporated under the vacuum. The resulting residue was purified by silica gel column chromatography to afford **13c**–**e**.

Ethyl 5-(adamantane-2-carboxamido)-1-(4-methoxybenzyl)-2-oxo-1,2-dihydroquinoline-3-carboxylate (13c) Following the general procedure **D**, esterification of ethylalcohol (0.005 mL, 0.09 mmol) affords **13c** (20.0 mg). Yield 38%; ^{1}H NMR (400 MHz, $CDCl_3$) δ 8.51 (1H, s), 7.56 (1H, s), 7.51–7.41 (2H, m), 7.39 (1H, d, *J* = 8.0 Hz), 7.15 (2H, t, *J* = 8.0 Hz), 6.80 (2H, d, *J* = 8.0 Hz), 5.48 (2H, s), 4.45–4.39 (2H, m), 3.74 (3H, s), 2.14 (3H, s), 2.06 (6H, s), 1.80–1.79 (6H, m), 1.43–1.39 (3H, m). ^{13}C NMR (125 MHz, $CDCl_3$) δ 206.85, 176.93, 164.96, 158.85, 158.70, 141.82, 138.29, 135.72, 133.21, 128.89, 128.07, 121.76, 119.08, 114.19, 113.91, 112.90, 61.61, 55.25, 46.21, 41.05, 39.34, 36.37, 30.91, 28.04, 14.30. MS

(ESI) *m/z*: 515.09 ([M+H]$^+$). HRMS (FAB) calcd for $C_{31}H_{34}N_2O_5$ [M]$^+$ 514.2468, found 514.2468. Purity 96%

Propyl 5-(adamantane-1-carboxamido)-1-(4-methoxybenzyl)-2-oxo-1,2-dihydroquinoline-3-carboxylate (13d) Following the general procedure **D**, esterification of 1-propanol (0.07 mL, 0.10 mmol) affords **13d** (10.0 mg). Yield 18%; ^{1}H NMR (400 MHz, $CDCl_3$) δ 8.51 (1H, s), 7.56 (1H, s), 7.52–7.44 (2H, m), 7.17–7.14 (3H, m), 6.82–6.80 (2H, m), 5.51 (2H, s), 4.35 (2H, t, *J* = 8.0 Hz), 3.76 (3H, s), 2.15 (3H, s), 2.07–2.03 (8H, m), 1.85–1.80 (6H, m), 1.08 (3H, t, *J* = 8.0 Hz). ^{13}C NMR (125 MHz, $CDCl_3$) δ 164.86, 158.87, 158.69, 141.76, 138.00, 135.74, 133.23, 128.05, 127.94, 121.86, 119.05, 114.21, 112.88, 67.21, 55.27, 46.10, 41.80, 39.40, 36.38, 28.11, 22.03, 10.60. MS (ESI) *m/z*: 529.07 ([M+H]$^+$). HRMS (FAB) calcd for $C_{32}H_{36}N_2O_5$ [M]$^+$ 528.2624, found 528.2624. Purity 95%

Isopropyl 5-(adamantane-1-carboxamido)-1-(4-methoxybenzyl)-2-oxo-1,2-dihydroquinoline-3-carboxylate (13e) Following the general procedure **D**, esterification of isopropylalcohol (0.07 mL, 0.10 mmol), affords **13e** (20.0 mg). Yield 37%; ^{1}H NMR (400 MHz, $CDCl_3$) δ 8.47 (1H, s), 7.56 (1H, s), 7.48 (1H, t, *J* = 8.0 Hz), 7.40 (1H, d, *J* = 8.0 Hz), 7.17–7.14 (3H, m), 6.82–6.80 (2H, m), 5.51 (2H, s), 5.32–5.26 (1H, m), 3.76 (3H, s), 2.16 (3H, s), 2.08–2.04 (9H, m), 1.85–1.75 (9H, m). MS (ESI) *m/z*: 529.07([M+H]$^+$). Purity 96%

General procedure E: For preparation of 13f and 13g

To a solution containing **13b** (1.0 equiv) in DMF, PyBop (2.0 equiv), appropriate amine derivative (1.5 equiv), and DIPEA (2.0 equiv) were added. After the reaction mixture was stirred for 12 h, it was concentrated and partitioned between water and ethyl acetate. The organic layer was dried over sodium sulfate, filtered and evaporated under the vacuum. The resulting residue was purified by silica gel column chromatography to afford **13f** and **13g**.

5-(Adamantane-1-carboxamido)-1-(4-methoxybenzyl)-N-methyl-2-oxo 1,2dihydroquinoline-3-carboxamide (13f) Following the general procedure **E**, coupling reaction of methylamine (33%, 0.003 mL, 0.01 mmol) affords **13f** (1.0 mg). Yield 20%; ^{1}H NMR (400 MHz, $CDCl_3$) δ 9.07 (2H, s), 7.85 (1H, s), 7.77 (1H, d, *J* = 8.0 Hz), 7.20 (1H, d, *J* = 8.0 Hz), 7.12 (2H, d, *J* = 8.0 Hz), 6.85 (2H, d, *J* = 8.0 Hz), 5.55 (2H, s), 3.04 (3H, d, *J* = 4.0 Hz), 2.15 (3H, s), 2.09–2.08 (6H, m), 1.81–1.79 (9H, m). MS (ESI) *m/z*: 500.11 ($[M+H]^+$). Purity 95%

5-(Adamantane-1-carboxamido)-1-(4-methoxybenzyl)-N,N-dimethyl-2-oxo-1,2 dihydroquinoline-3-carboxamide (13g) Following the general procedure **E**, coupling reaction of dimethylamine (0.002 mL, 0.01 mmol) affords **13g** (2.0 mg). Yield 38%; ^{1}H NMR (400 MHz, $CDCl_3$) δ 7.89 (1H, s), 7.70 (1H, s), 7.41 (2H, d, *J* = 8.0 Hz), 7.13 (3H, t, *J* = 8.0 Hz), 6.80 (2H, d, *J* = 8.0 Hz), 5.45 (2H, s), 3.76 (3H, s), 3.17 (3H, s), 3.01 (3H, s), 2.14 (3H, s), 2.04–2.00 (6H, m), 1.81–1.79 (6H, m). MS (ESI) *m/z*: 514.15 ($[M+H]^+$). Purity 99%

General procedure F: For preparation of 14a and 14b

A solution containing compound **9a**[38] (1.0 equiv) or **9b**[32] (1.0 equiv) in 1,2-DCE, and $POCl_3$ (2.0 equiv) were stirred at 80 ^oC for 12 h. The solvent and remained reagents were evaporated to afford **14a** and **14b**.

2-Chloro-5-nitroquinoline (14a)[43] Following the general procedure **F**, chlorination of **9a** (100.0 mg, 0.50 mmol) with $POCl_3$ (0.09 mL, 1.0 mmol) affords **14a** (78.0 mg). Yield 75%.

Methyl 2-chloro-5-nitroquinoline-3-carboxylate (14b) Following the general procedure **F**, chlorination of compound **9b** (100.0 mg, 0.40 mmol) with $POCl_3$ (0.007 mL, 0.80 mmol) affords **14b** (88.0 mg). Yield 82%; ^1H NMR (400 MHz, $CDCl_3$) δ 8.78 (1H, s), 7.60 (1H, t, *J* = 8.0 Hz), 7.43–7.40 (1H, m), 6.80 (1H, dd, *J* = 8.0 Hz, 8.0 Hz), 3.99 (3H, s). MS (ESI) *m/z*: 265.13 ($[M-H]^-$).

General procedure G: For preparation of 17a–g and 17i

Compound **16c** (1.0 equiv), appropriate boronic acid derivative (1.1 equiv), 2 M Na_2CO_3 in water (3.0 equiv) and $Pd(PPh_3)_4$ (0.1 equiv) were dissolved in 1,4-dioxane. After the reaction mixture was refluxed under argon gas for 3 h at 80 ^oC, it was concentrated, it was partitioned between water and ethyl acetate. The organic layer was dried over sodium sulfate, filtered and evaporated under the vacuum. The resulting residue was purified by silica gel column chromatography to afford **17a–g** and **17i**.

2-(Adamantan-1-yl)-N-(2-phenylquinolin-5-yl)acetamide (17a) Following the general procedure **G**, suzuki coupling reaction of phenylboronic acid (1.80 mg, 0.01 mmol) in 1,4-dioxane affords **17a** (3.0 mg). Yield 54%; ^{1}H NMR (400 MHz, $CDCl_3$) δ 8.11 (1H, d, *J* = 8.0 Hz), 7.93 (1H, d, *J* = 8.0 Hz), 7.89 (1H, d, *J* = 8.0 Hz), 7.69–7.63 (2H, m), 7.57–7.50 (2H, m), 7.49–7.42 (2H, m), 7.40 (1H, d, *J* = 8.0 Hz), 7.31 (1H, s), 2.27 (2H, m), 2.18 (1H, s), 2.04 (1H, s), 1.79–1.63 (13H, m). MS (ESI) *m/z*: 395.15 ([M-H]$^-$). Purity 97%

2-(Adamantan-1-yl)-N-(2-(4-methoxyphenyl)quinolin-5-yl)acetamide (17b) Following the general procedure **G**, suzuki coupling reaction of (4-methoxyphenyl)boronic acid (2.4 mg, 0.01 mmol) in 1,4-dioxane affords **17b** (3.0 mg). Yield 51%; ^{1}H NMR (400 MHz, $CDCl_3$) δ 8.14 (1H, d, *J* = 8.0 Hz), 7.90 (1H, d, *J* = 8.0 Hz), 7.82 (1H, d, *J* = 8.0 Hz), 7.71 (1H, t, *J* = 8.0 Hz), 7.69–7.59 (1H, m), 7.57–7.50 (1H, m), 7.49–7.43 (1H, m), 7.40 (1H, d, *J* = 8.0 Hz), 7.33 (1H, s), 3.77 (3H, s), 2.23 (2H, s), 2.02 (3H, s), 1.84–1.60 (13H, m). ^{13}C NMR (125 MHz, $CDCl_3$) δ 128.89, 115.98, 114.94, 114.13, 65.27, 55.31, 42.62, 41.93, 36.74, 33.51, 31.89, 29.69, 29.35, 28.66, 23.36, 22.68, 14.10, 11.01. MS (ESI) *m/z*: 425.23 ([M-H]$^-$). Purity 96%

2-(Adamantan-1-yl)-N-(2-(4-hydroxyphenyl)quinolin-5-yl)acetamide (17c) Following the general procedure **G**, suzuki coupling reaction of (4-hydroxyphenyl)boronic acid (1.9 mg, 0.01 mmol) in 1,4-dioxane affords **17c** (2.0 mg). Yield 34%; ^{1}H NMR (400 MHz, DMSO-d_6) δ 9.85 (1H, s), 8.43 (1H, d, *J* = 8.0 Hz), 8.11 (2H, d, *J* = 8.0 Hz), 8.06 (1H, d, *J* = 8.0 Hz), 7.69–7.62 (2H, m), 6.87 (2H, d, *J* = 8.0 Hz), 6.51 (1H, s), 2.21 (2H, s), 1.93 (3H, s), 1.72–1.54 (12H, m). ^{13}C NMR (125 MHz, DMSO-d_6) δ 170.23, 159.60, 156.23, 150.16, 148.38,

134.31, 133.58, 132.74, 132.70, 132.47, 129.70, 129.22, 129.14, 127.43, 126.12, 121.58, 121.04, 117.09, 50.77, 42.58, 36.96, 33.18, 28.58. MS (ESI) *m/z*: 413.09 ($[M+H]^+$). HRMS (ESI): calcd for $C_{27}H_{28}N_2O_2$ $[M+H]^+$ 412.2313, found. 412.2313. Purity 96%

2-(Adamantan-1-yl)-N-(2-(3-hydroxyphenyl)quinolin-5-yl)acetamide (17d) Following the general procedure **G**, suzuki coupling reaction of (3-hydroxyphenyl)boronic acid (1.9 mg, 0.01 mmol) in 1,4-dioxane affords **17d** (2.0 mg). Yield 34%; ^{1}H NMR (400 MHz, $CDCl_3$) δ 8.30 (1H, d, *J* = 8.0 Hz), 8.07 (1H, d, *J* = 8.0 Hz), 7.97–7.82 (3H, m), 7.72 (1H, t, *J* = 8.0 Hz), 7.41–7.31 (2H, m), 7.09 (1H, d, *J* = 8.0 Hz), 6.97 (1H, t, *J* = 8.0 Hz), 2.28 (2H, s), 2.18 (1H, s), 2.04 (1H, s), 1.79–1.63 (13H, m). MS (ESI) *m/z*: 413.00 ($[M+H]^+$). Purity 98%

2-(Adamantan-1-yl)-N-(2-(2-hydroxyphenyl)quinolin-5-yl)acetamide (17e) Following the general procedure **G**, suzuki coupling reaction of (2-hydroxyphenyl)boronic acid (1.9 mg, 0.01 mmol) in 1,4-dioxane affords **17e** (2.0 mg). Yield 34%; ^{1}H NMR (400 MHz, $CDCl_3$) δ 8.23 (1H, d, *J* = 8.0 Hz), 8.02 (1H, d, *J* = 8.0 Hz), 7.85 (2H, d, *J* = 8.0 Hz), 7.74–7.63 (3H, m), 7.42–7.35 (2H, m), 6.99–6.90 (1H, m), 2.29 (2H, s), 2.18 (1H, s), 2.04 (1H, s), 1.79–1.63 (13H, m). MS (ESI) *m/z*: 413.00 ($[M+H]^+$). Purity 95%

2-(Adamantan-1-yl)-N-(2-(4-chlorophenyl)quinolin-5-yl)acetamide (17f) Following the general procedure **G**, suzuki coupling reaction of (4-chlorophenyl)boronic acid (2.5 mg, 0.01 mmol) in 1,4-dioxane affords **17f** (3.0 mg). Yield 49%; ^{1}H NMR (400 MHz, $CDCl_3$) δ 8.14 (1H, d, *J* = 8.0 Hz), 7.90 (1H, d, *J* = 8.0 Hz), 7.82 (1H, d, *J* = 8.0 Hz), 7.69–7.61 (2H, m), 7.57–7.51 (2H, m), 7.49–7.44 (1H, m), 7.41 (1H, d, *J* = 8.0 Hz), 7.33 (1H, s), 2.25 (5H, m),

2.16–1.24 (12H, m). MS (ESI) *m/z*: 431.08 ($[M+H]^+$). Purity 96%

2-(Adamantan-1-yl)-N-(2-(4-nitrophenyl)quinolin-5-yl)acetamide (17g) Following the general procedure **G**, suzuki coupling reaction of (4-nitrophenyl)boronic acid (2.5 mg, 0.01 mmol) in 1,4-dioxane affords **17g** (3.0 mg). Yield 48%; ^{1}H NMR (400 MHz, DMSO-d_6) δ 8.66 (1H, d, *J* = 8.0 Hz), 8.59 (2H, d, *J* = 8.0 Hz), 8.42 (2H, d, *J* = 8.0 Hz), 8.36 (1H, d, *J* = 8.0 Hz), 7.96 (1H, d, *J* = 8.0 Hz), 7.89–7.77 (2H, m), 2.27 (2H, s), 1.94 (3H, s), 1.74–1.53 (12H, m). ^{13}C NMR (125 MHz, DMSO-d_6) δ 170.32, 154.04, 148.55, 148.40, 144.74, 134.44, 133.68, 130.47, 128.92, 126.62, 124.54, 122.52, 122.37, 119.00, 79.52, 50.75, 49.07, 42.61, 36.88, 33.26, 31.16, 28.55. MS (ESI) *m/z*: 440.00 ($[M-H]^-$). Purity 95%

4-(5-(2-(Adamantan-1-yl)acetamido)quinolin-2-yl)benzoic acid (17i) Following the general procedure **G**, suzuki coupling reaction of 4-boronobenzoic acid (2.3 mg, 0.01 mmol) in 1,4-dioxane affords **17i** (2.5 mg). Yield 40%; ^{1}H NMR (400 MHz, DMSO-d_6) δ 9.91 (1H, s), 8.53 (1H, d, *J* = 8.0 Hz), 8.19 (3H, t, *J* = 8.0 Hz), 7.99 (2H, d, *J* = 8.0 Hz), 7.85 (1H, d, *J* = 8.0 Hz), 7.76–7.68 (2H, m), 2.22 (2H, s), 1.93 (3H, s), 1.82 (1H, s), 1.74–1.53 (9H, m), 1.19 (2H, s). MS (ESI) *m/z*: 441.18 ($[M+H]^+$). Purity 97%

For preparation of methyl 4-(5-(2-(adamantan-1-yl)acetamido)quinolin-2-yl)benzoate (17j) CH_3I (1.2 equiv) was added to **17i** in DMF. After reaction mixture was stirred for 1 h, it was partitioned between a water and ethyl acetate. The organic layer was dried over sodium sulfate, filtered and evaporated under the vacuum. The resulting residue was purified by silica gel column chromatography to afford **17j**. Yield 53%; ^{1}H NMR (400 MHz, $CDCl_3$) δ 8.32–

8.16 (5H, m), 8.05 (1H, d, *J* = 8.0 Hz), 7.95 (1H, d, *J* = 8.0 Hz), 7.88 (1H, d, *J* = 8.0 Hz), 7.75 (1H, d, *J* = 8.0 Hz), 7.37 (1H, s), 3.97 (3H, s), 2.19 (2H, s), 2.05 (3H, s), 1.80–1.68 (12H, m). MS (ESI) *m/z*: 453.16 ([M-H]$^-$). Purity 95%

For preparation of 2-(adamantan-1-yl)-N-(2-(4-(hydroxymethyl)phenyl)quinolin-5-yl)acetamide (17k) Compound **17j** was dissolved in distilled THF and 1.0 M LAH in THF (1.2 equiv) was slowly added at 0 ^oC. After the reaction mixture was stirred for 9 h, remained LAH was carefully quenched by ammonium chloride. After the reaction mixture was concentrated, it was partitioned between ethyl acetate and ammonium chloride. The organic layer was dried over sodium sulfate, filtered and evaporated under the vacuum. The resulting residue was purified by silica gel column chromatography to afford **17k**. Yield 15%; ^1H NMR (400MHz, $CDCl_3$) δ 8.25 (1H, d, *J* = 8.0 Hz), 8.18 (2H, d, *J* = 8.0 Hz), 8.04 (1H, d, *J* = 8.0 Hz), 7.92 (1H, d, *J* = 8.0 Hz), 7.86 (1H, d, *J* = 8.0 Hz), 7.72 (1H, t, *J* = 8.0 Hz), 7.53 (2H, d, *J* = 8.0 Hz), 7.37 (1H, s), 6.79 (1H, d, *J* = 8.0 Hz), 4.80 (2H, s), 2.28 (2H, s), 2.04 (2H, s), 1.80–1.65 (13H, m). MS (ESI) *m/z*: 427.17 ([M+H]$^+$). ^{13}C NMR (125 MHz, DMSO-d_6) δ 145.01, 144.98, 134.54, 133.75, 132.74, 132.59, 132.04, 131.95, 129.38, 129.25, 127.50, 127.28, 125.90, 63.43, 63.11, 42.73, 36.97, 33.27, 28.63. HRMS (ESI): calcd for $C_{28}H_{30}N_2O_2$ $[M+H]^+$ 427.2380, found. 427.2354. Purity 98%

4.2. Biological methods.

4.2.1. In-vitro Assay for the Measurement of Ethidium Bromide Accumulation in Human HEK293-P2X7 cells[31]

To assess the SAR of a novel series of substituted quinolinone derivatives, these compounds were evaluated on 2’(3’)-O-(4-benzoylbenzoyl)-ATP (BzATP)-stimulated ethidium ion

accumulation in *h*P2X7-expressing HEK293 cells, as described.[44,45] Shortly, HEK293 cells were stably transfected, using Lipofectamine, with the human P2X7R cDNA in the pcDNA3.1 vector (Invitrogen), following the manufacturer's instructions. These stably transfected cells were maintained in a humidified atmosphere containing 5% CO_2 at 37 °C in DMEM supplemented with 10% FBS, 2 mM L-glutamine, and antibiotics (50 U/mL penicillin and 50 μg/mL streptomycin) and subcultured three times a week. Activation of P2X7R-associated pore formation was observed using a fluorescence plate reader by measuring the cellular uptake of ethidium in HEK293-P2X7 cells, as represented previously.[31] 1X PBS buffer consisting of 137 mM NaCl, 2.7 mM KCl, 10 mM Na_2HPO_4, 2 mM KH_2PO_4 is used for washing of HEK293-P2X7 cells in the growth medium and was removed before performing the assay. All experiments were performed at room temperature, and the final assay volume was 100 μL. The cells of 2.5×10^6 cells/mL were replaced with an assay solution consisting (in millimolar) of HEPES 10, N-methyl-Dglucamine 5, KCl 5.6, D-glucose 10, and $CaCl_2$ 0.5 (pH 7.4) and supplemented with either 280 mM sucrose or 140 mM NaCl. To determine the IC_{50} values of the quinolinone and quinoline derivatives, the reference compound **1** (KN-62) and **2** (AZD9056), these compounds were added to cells at different doses with BzATP. After incubation for 2 h, ethidium dye uptake was detected by measuring the fluorescence with a plate CHAMELEON™ multitechnology plate reader (excitation wavelength of 530 nm and emission wavelength of 590 nm). The results are indicated as percentages relative to the maximum accumulation of ethidium bromide when stimulated with BzATP only, and the IC_{50} values were measured using nonlinear regression analysis (i.e., percentage accumulation of ethidium bromide *vs* compound concentration).

4.2.2. In-vitro Assay for the Measurement of Enzyme-Linked Immunosorbent of Human IL-1β in Differentiated THP-1 cells[31]

THP-1 cells were maintained in suspension culture at a density of 5×10^4 to 1×10^6 cells/mL in RPMI 1640 medium supplemented with 10% FBS, 2 mM L-glutamine, penicillin (100 U/mL), and streptomycin (100 μg/mL). These cells were incubated at 37 °C in a humidified atmosphere containing 5% CO_2 and subcultured twice a week. All experiments were performed at room temperature, and the final assay volume was 150 μL. THP-1 cells of 1.5×10^5 cells/150 μL/well were plated onto 96-well plates. To differentiate THP-1 cells into macrophages, 25 ng/mL LPS and 10 ng/mL IFN-γ were treated to the cells for 4 h. Differentiated cells having an increased adherent character were incubated with various concentrations of quinolinone and quinolone derivatives, the reference compound **1** (KN-62) and **2** (AZD9056) for 30 min and then with 1 mM BzATP for an additional 30 min. Next, supernatants were collected and stored at −70 °C. The level of IL-1β was determined by ELISA using anti-human IL-1β antibody as a capture antibody and a biotinylated antihuman IL-1β antibody as a detection antibody (eBioscience). Recombinant human IL-1β was used as a standard (eBioscience). ELISA was conducted following the manufacturer's instructions. These results are indicated as a percentage of the maximal BzATP in terms of the absolute amount of IL-1β released, and the IC_{50} values were measured using nonlinear regression analysis (i.e., percentage IL-1β release *vs* compound concentration). A basal level of IL-1β was subtracted from the data in the normalization calculations.

4.2.3. In-vitro Selectivity test for other P2X Receptors[31]

Calcium influx assays were performed as previously described.[46] The compounds (**16c**, **16e** and **17b**) were initially tested at a concentration of 10 μM and 1 μM for their potency to inhibit ATP-induced calcium influx in 1321N1 astrocytoma cells stably transfected with one

of the human P2X receptor subtypes: P2X1, P2X2, P2X3, or P2X4, respectively. For **17b**, full concentration–response curves were determined and IC_{50} values were calculated. An ATP concentration which caused ~80% of the maximal effect was used for receptor stimulation.

4.2.4. Cell culture

TS15-88 glioblastoma cells were cultured in DMEM/F12 (Corning, New York, PA, USA) media supplemented with B-27 (Thermo Fisher Scientific), 20 ng/ml of human EFG (Sigma), 20 ng/ml of human βFGF (Sigma) and penicillin-streptomycin (Thermo Fisher Scientific) in a 37 °C, 5% CO_2 humidifier.

4.2.5. MTS assay

TS15-88 cells were seeded in a 96-well plate at a density of 5.0 x 10^3 cells/100 µL of complete media/well and the cells were incubated for 24 h at 37 °C before drug treatments. Cells were treated with or without tested drug compounds for 5 days at 37 °C. After treatment, 20 µL of MTS solution (Promega) was added to each well, and 96-well plates were incubated for 4 h in a 37 °C, 5% CO_2 humidifier. The wavelength absorbance of each well was measured using an Epoch microplate spectrophotometer at 490 nm (BioTek instruments).

4.2.6. Neurosphere formation assay

TS15-88 cells were seeded in a 96-well plate at a density of 1.0 x 10^3 cells/100 µL of complete media/well, and the cells were incubated for 24 h at 37 °C before drug treatments.

Cells were treated with or without tested drug compounds for 5 days at 37 °C. After 5 days, images of each well were captured using a Nikon Eclipse Ti microscope (Nikon). The total sphere area was analyzed using the Image J software.

4.2.7. RNA isolation and cDNA preparation

After cells were treated for 3 days with drug, drug treated and untreated control cells were harvested by simple centrifugation. TRIzol (Thermo Fisher Scientific) was added onto the pellet of each sample to homogenize the samples. RNA extraction was followed by the manufacturer's protocol. Then, 1 μg of extracted total RNA was used for the synthesis of cDNA using Reverse Transcription System (Promega) in a volume of 20 μL. Detailed cDNA synthesis procedures were achieved following the manufacturer's protocol. After 30 min of cDNA synthesis in 42 °C, samples were incubated in 95 °C for 5 min to inactivate. Synthesized cDNA samples were diluted to 350 μL.

4.2.8. Quantitative Real-time PCR

A total of 20 μL of PCR reaction with 1 μL of template and 10 μL of PowerUp™ SYBR® Green Master Mix (Thermo Fisher Scientific) was used in an Applied Biosystems 7500 Real-Time PCR Instrument System (Thermo Fisher Scientific). 18S was used as an endogenous control in the comparative CT method. All experiments were performed in quadruplicate. Each PCR primer sequence was used for qRT-PCR analysis, as shown in figure 5, and all primer sets were tested. Only single amplicons were observed.

4.2.9. qRT-PCR primer

Gene	Forward primer	Reverse primer
18S	CGG CTA CCA CAT CCA AGG AA	TTT TCG TCA CTA CCT CCC CG
MYC	GGC TCC TGG CAA AAG GTC A	CTG CGT AGT TGT GCT GAT GT
POU5F1	GGG CTC TCC CAT GCA TTC AA	CAC CTT CCC TCC AAC CAG TT
SOX2	TCG GCA GAC TGA TTC AAA TAA TAC AG	CCA TGC AGG TTG ACA CCG TTG
CD133	AAG CTG GAC CCA TTG GCA TT	AAA GTA TCT TCT GGG AAA TCA CGC

4.2.10. Blood-Brain Barrier (BBB) Permeability

4.2.10.1. Materials and Methods

Animals: adult male zebrafish of the *Danio rerio* strain, weighing approximately 0.26 g, were used in this study. The animals were maintained under the 14/10 h light/dark cycle at 28 ± 1 °C in an aquatic recirculation system (Genomic Design Bioengineering Company, Daejeon, Korea). They were fed thrice daily with *artemia naupli* and fasted overnight before the experiments. All experimental protocols involving the animals used in this study were reviewed and approved by the Animal Care and Use Committee of the Korea Research Institute of Chemical Technology, according to the National Institutes of Health Publication Number 85-23, (revised 1985) in Principles of Laboratory Animal Care.

4.2.10.2. Animal Experiments: Oral Administration of chemicals to Zebrafish

Three zebrafish were randomly assigned from the water tank based on the designated time, and the dosing method (oral gavage) was applied as described previously. Briefly, a moistened sponge was placed on the flat surface of the 1 L water tank, and the adult fish were slightly anesthetized with 0.4% tricaine. Each fish was moved on to the sponge in a vertical position, following which the dosing solution was orally administered with chemical (10 mg/kg) using a micropipette connected to a SILASTIC laboratory tubing (internal diameter, 0.64 mm; outside diameter, 1.19 mm). The fish were then individually placed into a tank of fresh water and incubated until sample collection. After 0.5 h, the fish were sacrificed and 2 µL of blood was carefully collected from the regions of the inferior vena cava and dorsal aorta using a micropipette with a heparinized tip. The brain samples were rinsed with cold saline and the wet-weights were determined. The samples were then placed in four volumes (w/v) of phosphate buffered saline (PBS, pH 7.4) and homogenized with a sonicator (Ultrasonic processor VCX-130, Sonics & Materials Inc, Newtown, CT, USA). The blood samples and brain homogenates were stored at −80 °C until further analysis.

4.2.10.3. Estimation of Brain to Blood Concentration Ratio in Zebrafish

The zebrafish were orally administered with each of the chemicals at 10 mg/kg optimized vehicle, and then incubated in the 1 L tank of fresh water as described earlier. After the fish were separately sacrificed 0.5 h after the dosing, the blood was collected and the brain was isolated as described earlier. The brain samples were rinsed with cold saline followed by wet-weight measurements. The samples were then placed in four volumes (w/v) of PBS (pH 7.4) and homogenized with an ultra-sonicator. The blood samples and brain homogenates were

stored at −80 °C until further analysis.

4.2.10.4. Analytical Procedure for the Determination of Compounds

The concentrations of each compound in the blood and brain homogenates were determined by a specific LC–MS/MS assay using disopyramide as an internal standard (IS). An aliquot (38 µL for blood or 36 µL for brain homogenate) of the IS solution (concentration 5 ng/mL in acetonitrile) was added to 2 µL of blood, or 4 µL of brain homogenate. After vortexing for 10 min, the extracts were centrifuged (13,000 rpm, 5 min, 4 °C). Next, 5 µL of the supernatant was injected onto the analytical column. Sample analyses were carried out with a 1200 series HPLC system (Agilent, Santa Clara, CA, USA) coupled to an Agilent 6460 triple quadruple mass spectrometry (Agilent Technologies, Santa Clara, CA, USA) and equipped with a turbo-electrospray interface in positive ionization mode for LC–MS/MS analysis. A mixture of acetonitrile and 10 mM ammonium formate (8:2, v/v) at a flow rate of 0.3 mL/min was used as the mobile phase. Separation was accomplished using a Kinetex C18 column (50 mm × 2.1 mm i.d., 2.6 µm; Phenomenex, USA) using a guard cartridge system (SecurityGuard C18; 4 mm × 20 mm i.d., Phenomenex, USA). Quantification was carried out using multiple reaction monitoring (MRM) at each optimized m/z values (data not shown). The optimized instrument conditions were as follows: source temperature, 350 °C; gas flow, 10 L/min; nebulizer, 45 psi; sheath gas temperature, 350 °C; sheath gas flow, 11 L/min). The peak areas for all components were automatically integrated using MassHunter Quantitative Analysis (Ver. B.06; Agilent Technologies).

4.2.10.5. Statistical Analysis

All data are expressed as the mean ± standard deviation (SD). Statistical analyses were performed using unpaired t-test. A value $p < 0.05$ was accepted as denoting a statistical significance.

4.2.10.6. Parallel artificial membrane permeability (PAMPA) assay

PAMPA assay was conducted by manufacturer's instruction (Pion, Inc, MA, USA). Briefly, test compound was diluted in donor buffer (pH 7.4) to be 50 μM and added 200 μL in lower bottom of 96 well transwell plate. Side to donor parts of transmembrane were coated with GIT lipid solution and added 150 μL acceptor buffer (pH 7.4) in upper part of transwell plate. After incubation for 4 h at 25 °C, each part of samples was measured with UV absorbance at wavelength between 250 nm and 498 nm and permeability rate was analyzed using Pion Pampa Explorer (ver 3.8).

4.2.10.7. In-vitro metabolic stability

This assay was performed by incubation of human and selected animal liver microsomes ((Rat liver microsomes: Cat# 452501, Corning), (Mouse liver microsomes: Cat# 452701, Corning) (Mixed Gender Pooled 150-donor Human liver microsomes: Cat# 452117, Corning)) at 37 °C with a test compound at a final concentration of 1 μM, in the presence of 0.5 mg/mL microsomal protein and NADPH regeneration system, in a total volume of 100 μL of 100 mM phosphate buffer, pH 7.4. The incubation started by the addition of NADPH regeneration system and terminated with 40 μL of ice-cold acetonitrile at 0 and 30 min. Precipitated proteins were removed by centrifugation at 10,000×g for 5 min at 4 °C. Aliquots of the

supernatant were injected onto an LC-MS/MS system. Incubations terminated prior to addition of NADPH regeneration system (time point 0 min) was used as standards, defined as 100%. Percent of the parent compound remaining is calculated by comparing peak areas.

4.2.10.8. Kinetic solubility assay

10 mM DMSO stock solution of compound was diluted with DMSO to be the concentration of 500 µM to 0.976563 µM solutions (12 wells) in 12 mL bio tube. 25 µM of each solution of 12 wells was taken and was diluted with water to make 500 µM solutions. Nephelostar was used with 150 µM X 3 times of each solution in 96 well plate using by Nepheolometry method.

4.2.10.9. Equilibrium solubility assay

10 µL of 50 mM stock dissolved in DMSO was added to 1 mL of pH 7.4 buffer containing PRISMA ™ HT and it was shaken at 25 ° C and 300 rpm for 16 h (n = 3). Reference sample was made by mixing pH 7.4 buffer of PRISMA™ HT and n-propanol with 50 mM DMSO stock solution. After shaking for 16 h, the mixture was filtered using PVDF filter, and the solution was measured its absorbance using the µSOL measurement program including the reference material to obtain the solubility value.

ACKNOWLEDGEMENTS

This research was supported by Basic Science Research Program through the National Research Foundation of Korea (NRF) funded by the Ministry of Science, ICT & Future

Planning (NRF-2015R1D1A4A01015910) and this research was supported by GIST-Caltech Research Collaboration grant funded by the GIST in 2017.

Supporting Information: Supporting information related to this article can be found at http://www.elsevier.com.

ABBREVIATION USED

LPS. lipopolysaccharides;

IFN. interferon;

MeOH. methanol;

$POCl_3$. phosphoryl chloride;

$SnCl_2$. tin (Ⅱ) chloride;

CH_3I. methyliodide;

DMF. dimethylformamide;

KOH. potassium hydroxide;

DMSO. dimethyl sulfoxide;

DCM. dichloromethane;

DIPEA. N,N-diisopropylethylamine;

HCl. hydrochloric acid;

DMAP. 4-dimethylaminopyridine;

EDC. 1-ethyl-3-(3-dimethylaminopropyl)carbodiimide;

PyBop. benzotriazol-1-yl-oxytripyrrolidinophosphonium hexafluorophosphate;

1,2-DCE. 1,2-dichloroethene;

EtOH. ethanol;

Na_2CO_3. sodium carbonate;

$Pd(PPh_3)_4$. tetrakis(triphenylphosphine)palladium (0);

LAH. lithium aluminum hydride;

NMR. nuclear magnetic resonance;

References

1. B.B. Fredholm, M.P. Abbracchio, G. Burnstock, G.R. Dubyak, T.K. Harden, K.A. Jacobson, U. Schwabe, M. Williams, Towards a revised nomenclature for P1 and P2 receptors. Trends pharmacol. Sci. 18 (1997) 79–82.

2. G. Burnstock, Purine and Pyrimidines. Cell. Mol Life Sci. 64 (2007) 1471–1483.

3. V. Ralevic, G. Burnstock, Receptors for Purines and Pyrimidines. Pharmacol. Rev. 50 (1998) 413–492.

4. B.S. Khakh, G. Burnstock, C. Kennedy, B.F. King, R.A. North, P. Séguéla, M. Voigt, P.P Humphrey, International Union of Pharmacology. XXIV. Current Status of the Nomenclature and Properties of P2X Receptors and Their Subunits. Pharmacol. Rev. 53 (2001) 107–118.

5. R.A. North, Molecular physiology of P2X Receptor. Physio. Rev. 82 (2002) 1013–1067.

6. X. Wang, G. Arcuino, T. Takano, J. Lin, W.G. Peng, P. Wan, P. Li, Q. Xu, Q.S. Liu, S.A. Goldman, M. Nedergaard, $P2X_7$ receptor inhibition improves recovery after spinal cord injury. Nat. Med. 10 (2004) 821–827.

7. A. Surprenant, F. Rassendran, E. Kawshima, R.A. North, G. Buell, The cytolytic P2Z receptor for extracellular ATP identified as a P2X receptor ($P2X_7$). Science. 272 (1996) 735–738.

8. O.R. Baricordi, D. Ferrari, L. Melchiorri, P. Chiozzi, S. Hanau, E. Chiari, M. Rubini, F. Di Virgilio, An ATP-activated channel is involved in mitogenic stimulation of human T lymphocytes. Blood. 87 (1996) 682–690.

9. S.D. Skaper, P. Debetto, P. Giusti, The $P2X_7$ Purinergic Receptor: From Physiology to Neurological Disorders. FASEB. J. 24 (2010) 337–345.

10. L. Narcisse, E. Scemes, Y. Zhao, S.C. Lee, C.F. Brosnan, The cytokine IL-1 beta transiently enhances $P2X(_7)$ receptor expression and function in human astrocytes. Glia. 49 (2005) 245–258.

11. M. Solle, J. Labasi, D.G. Perregaux, E. Stam, N. Petrushova, B.H. Koller, R.J. Griffiths, C.A. Gabel, Altered cytokine production in mice lacking $P2X(_7)$ receptors. J. Biol. Chem. 276 (2001) 125–132.

12. J.E. Sims, D.E. Smith, The IL-1 family: regulators of immunity. Nature Reviews Immunity. 10 (2010) 89–102.

13. T.H. Steinberg, J.F. Hiken, P2 receptors in macrophage fusion and osteoclast formation. Purinergic Signal. 3 (2007) 53–57.

14. D. Ferrari, P. Chiozzi, S. Falzoni, M. Dal Susino, G. Collo, G. Buell, F. Di Virgilio, ATP-mediated cytotoxicity in microglial cells. Neuropharmacology. 36 (1997) 1295–1301.

15. R. Le Feuvre, D. Brough, N. Rothwell, Extracellular ATP and $P2X_7$ receptors in neurodegeneration. Eur. J. Pharmacol. 447 (2002) 261–269.

16. D.L. Donnelly-Roberts, M.F. Jarvis, Discovery of $P2X_7$ receptor-selective antagonists offers new insights into $P2X_7$ receptor function and indicates a role in chronic pain states. Br. J. Pharmacol. 151 (2007) 571–579.

17. I.P. Chessell, J.P. Hatcher, C. Bountra, A.D. Michel, J.P. Hughes, P. Green, J. Egerton, M. Murfin, J. Richardson, W.L. Peck, C.B. Grahames, M.A. Casula, Y. Yiangou, R. Birch, P. Anand, G.N. Buell, Disruption of the $P2X_7$ purinoceptor gene abolishes chronic inflammatory and neuropathic pain. Pain. 114 (2005) 386–396.

18. F. Di virgilio, S. Falzoni, C. Mutini, J.M. Sanz, P. Chiozzi, Purinergic $P2X_7$ receptor: A pivotal role in inflammation and immunomodulation. Drug develop. Res. 45 (1998) 207–213.

19. (a) X.J. Zhang, G.G. Zheng, X.T. Ma, Y.H. Yang, G. Li, Q. Rao, K. Nie, K.F. Wu, Expression of P2X7 in human hematopoietic cell lines and leukemia patients. Leuk. Res. 28 (2004) 1313−1322. (b) T. Deli, N. Varga, A. Adám, I. Kenessey, E. Rásó, L.G. Puskás, J. Tóvári, J. Fodor, M. Fehér, G.P. Szigeti, L. Csernoch, J. Tímár, Functional genomics of calcium channels in human melanoma cells. Int. J. Cancer. 121 (2007) 55−65. (c) M. Slater, S. Danieletto, A. Gidley-Baird, L.C. Teh, J.A. Barden, Early prostate cancer detected using expression of non-functional cytolytic P2X7 receptors. Histopathology. 44 (2004) 206−215. (d) L. Raffaghello, P. Chiozzi, S. Falzoni, F. Di Virgilio, V. Pistoia, The P2X7 receptor sustains the growth of human neuroblastoma cells through a substance P-dependent mechanism. Cancer Res. 66 (2006) 907−914. (e) E. Adinolfi, L. Melchiorri, S. Falzoni, P. Chiozzi, A. Morelli, A. Tieghi, A. Cuneo, G. Castoldi, F. Di Virgilio, O.R. Baricordi, P2X7 receptor expression in evolutive and indolent forms of chronic B lymphocytic leukemia. Blood. 99 (2002) 706−708.

20. (a) J. Xia, X. Yu, L. Tang, G. Li, T. He, P2X7 receptor stimulates breast cancer cell invasion and migration via the AKT pathway. Oncol. Rep. 34 (2015) 103−110. (b) T.A. Martin, L. Ye, A.J. Sanders, J. Lane, W.G. Jiang, Cancer invasion and metastasis: molecular and cellular perspective. Landes Bioscience. (2013) 1−63. (c) F.G. Vázquez-Cuevas, A.S. Martínez-Ramírez, L. Robles-Martínez, E. Garay, A. García-Carrancá, D. Pérez-Montiel, C. Castañeda-García, R.O. Arellano, Paracrine stimulation of P2X7 receptor by ATP activates a proliferative pathway in ovarian carcinoma cells. J. Cell. Biochem. 115 (2014) 1955−1966. (d) A. Ghalali, F. Wiklund, H. Zheng, U. Stenius, J. Högberg, Atorvastatin prevents ATP-driven invasiveness via P2X7 and EHBP1 signaling in PTEN-expressing prostate cancer cells. Carcinogenesis. 35 (2014) 1547−1555.

21. (a) M. Monif, T.J O'Brien, K.J. Drummond, C.A. Reid, S.V. Liubinas, D.A. Williams, P2X7 receptors are a potential novel target for anti-glioma therapies. Journal of Inflammation. 11 (2014). (b) M.P. Gehring, F. Kipper, N.F. Nicoletti, N.D. Sperotto, R. Zanin, A.S. Tamajusuku, D.G. Flores, L. Meurer, R. Roesler, A.B. Filho, G. Lenz, M.M. Campos, F.B. Morrone. P2X7 receptor as predictor gene for glioma radiosensitivity and median survival. Int J Biochem Cell Biol. 68 (2015) 92−100.

22. (a) P. Flores Ledur, E. Schlee Villodre, R. Paulus, L. Almeida Cruz, D. Grazzana Flores, G. Lenz, Extracellular ATP reduces tumor sphere growth and cancer stem cell population in glioblastoma cells. Purinergic Signal. 8 (2012) 39–48. (b) M. Monif, C.A. Reid, K.L. Powell, M.L. Smart, D.A.Williams, The P2X7 Receptor Drives Microglial Activation and Proliferation: A Trophic Role for P2X7R Pore. J. Neurosci. 29 (2009) 3781–3791

23. (a) B.D. Humphreys, C. Virginio, A. Surprenant, J. Rice, G.R. Dubyak, Isoquinolines as antagonists of the $P2X_7$ nucleotide receptor: High selectivity for the human versus rat receptor homologues. Mol. Pharmacol. 54 (1998) 22–32. (b) C.E. Gargett, J.S.

Wiley, The Isoquinoline Derivative KN-62 a Potent Antagonist of the P2Z-receptor of Human Lymphocytes. Br. J. Pharmacol. 120 (1997) 1483–1490.

24. (a) E.C. Keystone, M.M. Wang, M. Layton, S. Hollis, I.B. McInnes, Clinical evaluation of the efficacy of the $P2X_7$ purinergic receptor antagonist AZD9056 on the signs and symptoms of rheumatoid arthritis in patients with active disease despite treatment with methotrexate or sulphasalazine. Ann Rheum Dis. 71 (2012) 1630–1635. (b) M. Furber, L. Alcaraz, J.E. Bent, A. Beyerbach, K. Bowers, M. Braddock, M.V. Caffrey, D. Cladingboel, J. Collington, D.K. Donald, M. Fagura, F. Ince, E.C. Kinchin, C. Laurent, M. Lawson, T.J. Luker, M.M. Mortimore, A.D. Pimm, R.J. Riley, N. Roberts, M. Robertson, J. Theaker, P.V. Thorne, R. Weaver, P. Webborn, P. Willis, Discovery of Potent and Selective Adamantane-based Small-molecule $P2X_7$ Receptor Antagonists/interleukin-1β Inhibitors. J. Med. Chem. 50 (2007) 5882–5885.

25. T.C. Stock, B.J. Bloom, N. Wei, S. Ishag, W. Park, X. Wang, P. Gupta, C.A. Mebus, Efficacy and safety of CE-224,535, an antagonist of P2X7 receptor, in treatment of patients with rheumatoid arthritis inadequately controlled by methotrexate. J Rheumatol. 39 (2012) 720–727.

26. D.W. Nelson, R.J. Gregg, M.E. Kort, A. Perez-Medrano, E.A. Voight, T. Wang, G. Grayson, M.T. Namovic, D.L. Donnelly-Roberts, W. Niforatos, P. Honore, M. Jarvis, C.R. Faltynek, W.A. Carroll, Structure-activity relationship studies on a series of novel, substituted 1-benzyl-5-phenyltetrazole $P2X_7$ antagonists. J. Med. Chem. 49 (2006) 3659–3666.

27. P. Honore, D. Donnelly-Roberts, M.T. Namovic, G. Hsieh, C.Z. Zhu, J.P. Mikusa, G. Hernandez, C. Zhong, D. Gauvin, P. Chandran, R. Harris, A.P. Medrano, W. Carroll, K. Marsh, J.P. Sullivan, C.R. Faltynek, M.F. Jarvis, A-740003 (N-(1-{[(cyanoimino)(5-quinolinylamino)methyl]amino}-2,2-dimethylpropyl)-2-(3,4-dimethoxyphenyl)acetamide, a novel and selective $P2X_7$ receptor antagonist dose-

dependently reduces neuropathic pain in the rat. J Pharmacol Exp Ther. 329 (2006) 1376–1385.

28. D.C. Broom, D.J. Matson, E. Bradshaw, M.E. Buck, R. Meade, S. Coombs, M. Matchett, K.K. Ford, W. Yu, J. Yuan, S.H. Sun, R. Ochoa, J.E. Krause, D.J. Wustrow, D.N. Cortright, Characterization of N-(adamantan-1-ylmethyl)-5-[(3R-amino-pyrrolidin-1-yl)methyl]-2-chloro-benzamide, a $P2X_7$ antagonist in animal models of pain and inflammation. J Pharmacol Exp Ther. 327 (2008) 620–633.

29. W.G. Lee, S.D. Lee, J.H. Cho, Y. Jung, J.H. Kim, T.T. Hien, K.W. Kang, H. Ko, Y.C. Kim, Structure−activity Relationships and Optimization of 3,5-Dichloropyridine Derivatives as Novel $P2X_7$ Receptor Antagonists. J. Med. Chem. 55 (2012) 3687−3698.

30. J.H. Park, G.E. Lee, S.D. Lee, T.T. Hien, S. Kim, J.W. Yang, J.H. Cho, H. Ko, S.C. Lim, Y.G. Kim, K.W. Kang, Y.C. Kim, Discovery of Novel 2,5-Dioxoimidazolidine-Based P2X7 Receptor Antagonists as Constrained Analogues of KN62. J. Med. Chem. 58 (2015) 2114−2134.

31. J.H. Park, D.R. Williams, J.H. Lee, S.D. Lee, J.H. Lee, H. Ko, G.E. Lee, S. Kim, J.M. Lee, A. Abdelrahman, C.E. Müller, D.W. Jung, Y.C. Kim, Potent Suppressive Effects of 1-Piperidinylimidazole Based Novel P2X7 Receptor Antagonists on Cancer Cell Migration and Invasion. J. Med. Chem. 59 (2016) 7410−7430

32. S.H. Kwak, M. Kim, S.D. Lee, H. You, Y.C. Kim, H. Ko, Solid-Phase Synthesis of Quinolinone Library. ACS Comb. Sci. 17 (2015) 60−69

33. (a) W. Kim, M.E. Zandoná, S.H. Kim, H.J. Kim, Oral disease-modifying treatments for multiple sclerosis. J Clin Neurol. 11 (2015) 9−19. (b) T. Tojo, G.W. Spears, K. Tsuji, H. Nishimura, T. Ogino, N. Seki, A. Sugiyama, M. Matsuo, Quinoline-3-carbothioamides and related compounds as novel immunomodulating agents. Bioorg. Med. Chem. Lett. 12 (2002) 2427−2430.

34. J.H. Noseworthy, J.S. Wolinsky, F.D. Lublin, J.N. Whitaker, A. Linde, P. Gjorstrup, H.C. Sullivan, North American linomide investigators: Linomide in relapsing and secondary progressive MS Part I: Trial design and clinical results. Neurology. 54 (2000) 1726−1733.

35. O. Nived, G. Sturfelt, B. Nilsson, B. Termander, P.O. Gunnarsson, K. Strandgarden, K.F. Wollheim, 1994: Clinical pilot study of roquinimex in patients with autoimmune disease. Int. J. Immunotherapy. 10 (1994) 49−59.

36. D.J. Gross, L. Weiss, I. Reibstein, G. Hedlund, E. Dahlén, M.J. Rapoport, S. Slavin, The immunomodulator linomide: Role in treatment and prevention of autoimmune diabetes mellitus. Int. Immunopharmacol. 1 (2001) 1131−1139.

37. S.H. Kwak, J.A. Kang, M. Kim, S.D. Lee, J.H. Park, S.G. Park, H. Ko, Y.C. Kim, Discovery and Structure-activity Relationship Studies of Quinolinone Derivatives as Potent IL-2 Suppressive Agents. Bioorg. Med. Chem. 24 (2016) 5357−5367.

38. R.A. Schumacher, A. Tehim, W. Xie, Preparation of pyrrolo[3,2-b]pyridine compounds as 5-HT6 receptor modulators for treatment of CNS disorders. PCT Int. Appl. 2010, WO 2010024980 A1.

39. (a) J.P.M. Lommerse, S.L. Price, R. Taylor, Hydrogen bonding of carbonyl, ether, and ester oxygen atoms with alkanol hydroxyl groups. J Comput Chem. 18 (1997) 757−774. (b) K.N. Vijayadas, R.V. Nair, R.L. Gawade, A.S. Kotmale, P. Prabhakaran, R.G. Gonnade, V.G. Puranik, P.R. Rajamohanan, G.J. Sanjayan, Ester vs. amide on folding: a case study with a 2-residue synthetic peptide. Org. Biomol. Chem. 11 **(**2013) 8348−8356.

40. (a) R. Evans, R. Ford, T. Thompson, P. Willis, Novel compounds. PCT Int. Appl. 2005, WO 2006059945. (b) R. Ford, T. Thompson, P. Willis, Derives de la quinoline et leur utilisation en therapie. PCT Int. Appl. 2004, WO 2005009968. (c) R. Evans, C. Eyssade, R. Ford, B. Martin, T. Thompson, P. Willis, New p2x7 receptor antagonists

and their use. PCT Int. Appl. 2004, WO 2004106305. (d) R. Ford, F. Leroux, M. Stocks, Novel adamantane derivatives. PCT Int. Appl. 2003, WO 2003080579.

41. T. Mosmann, Rapid Colorimetric Assay for Cellular Growth and Survival: Application to Proliferation and Cytotoxicity Assays. J Immunol Methods. 65 (1983) 55−63.

42. K. Pushkar, C. Girish Hari, S. Vijaykumar, B. Rakesh Kumar, K. Krishna Tulasi, S. Razia, R. Pallavi, O. Srinivas, C. Kiranam. Oral dosing in adult zebrafish: Proof-of-concept using pharmacokinetics and pharmacological evaluation of carbamazepine. Pharmacological Reports 66 (2014) 179−183.

43. T. Kiyoto, T. Tanaka, Y. Tsutsui, J. Ando, M. Motono, Y. Kawaguchi, T. Noguchi, Y. Ushiki, F. Ushiyama, H. Urabe, Novel nitrogenated heterocyclic compound and salt thereof. EP1900732 A1.

44. S.Y. Lee, S. Jo, G.E. Lee, L.S. Jeong, Y.C. Kim, C.S. Park, Establishment of an Assay for $P2X_7$ Receptor-mediated Cell Death. Mol. Cells. 22 (2006) 198−202.

45. A.D. Michel, M. Xing, K.M. Thompson, C.A. Jones, P.P Humphrey, Decavanadate, a P2X Receptor Antagonist, and Its Use to Study Ligand Interactions with $P2X_7$ Receptors. Eur. J. Pharmacol. 534 (2006) 19−29.

46. V. Hernandez-Olmos, A. Abdelrahman, A. El-Tayeb, D. Freudendahl, S. Weinhausen, C.E. Müller, N-substituted phenoxazine and acridone derivatives: structure-activity relationships of potent P2X4 receptor antagonists. J. Med. Chem. 26 (2012) 9576−9588.

47. M.U. Kassack, K. Braun, M. Ganso, H. Ullmann, P. Nickel, B. Böing, G. Müller, G. Lambrecht, Structure-activity relationships of analogues of NF449 confirm NF449 as

the most potent and selective known P2X1 receptor antagonist. Eur. J. Med. Chem. 39 (2004) 345−357.

48. Y. Baqi, R. Hausmann, C. Rosefort, J. Rettinger, G. Schmalzing, C.E. Müller, Discovery of potent competitive antagonists and positive modulators of the P2X2 receptor. J. Med. Chem. 54 (2011) 817−830.

49. R. Hausmann, J. Rettinger, Z. Gerevich, S. Meis, M.U. Kassack, P. Illes, G. Lambrecht, G. Schmalzing, The suramin analog 4 ,4′ , 4 ″ , 4 ‴ - (c a r b o n y l b i s (i m i n o - 5 , 1 , 3 - b e n z e n e t r i y l b i s (carbonylimino)))tetra-kis benzenesulfonic acid (NF110) potently blocks P2X3 receptors: subtype selectivity is determined by location of sulfonic acid groups. Mol. Pharmacol. 69 (2006) 2058−2067.

50. D. Donnelly-Roberts, S. Mc Garaughty, C.C. Shieh, P. Honore, M.F. Jarvis, Painful purinergic receptors. J. Pharmacol. Exp. Ther. 324 (2008) 409−415.

51. E.H. Kerns, L. Di, G.T. Carter, In Vitro Solubility Assays in Drug Discovery. Curr. Drug. Metab. 9 (2008) 879−885.

Legends to Figures

Figure 1. Structure of P2X7R antagonists.

Figure 2. MTS assay.

After 24 h and 72 h treatment of drug, cell viability was measured by MTS assay. Values were normalized by the DMSO treated group and all values represent the mean viability of cells ± SEM (n = 3). ($p<0.05$,*; $0.005<p<0.05$, **; $p<0.005$, ***)

Figure 3. Neurosphere formation assay (sphere size on TS15-88 glioblastoma cells).

All images are x 40 magnification with scale bar = 50 μm. Quantification of the total sphere sizes that were formed from single-cell was performed after 5 days treatments with respective drugs (n = 3).

Figure 4. Neurosphere formation assay of TS15-88 glioblastoma cells.

After 5 days drug treatment, total sphere area of each well was measured with Image J software. Values were normalized by the total sphere area of DMSO treated group and all bar graphs represent the mean of total sphere area ± SEM (n = 3). ($p<0.05$,*; $0.005<p<0.05$, **; $p<0.005$, ***)

Figure 5. Quantitative RT-PCR result after **16c** treatment.

After 72 h treatment of compound **16c**, relative amount of mRNA level was measured by quantitative RT-PCR (qRT-PCR). POU5F1, SOX2, MYC and CD133 expression with untreated (white bar) and treated (black bar) group in TS15-88 glioblastoma cells was

analyzed. Each bar represented mean expression ± SEM of relative mRNA levels of gene and 18S was used as endogenous control (n = 4). ($p<0.05$,*; $0.005<p<0.05$, **; $p<0.005$, ***)

Figure 6. Concentration of compound **16c** in blood and brain tissue (n = 3).

Legends and Reaction Conditions of Schemes

Scheme 1. Synthesis of quinolinone derivatives.

a) i) $SnCl_2$, EtOH, argon gas, 80 ^oC, 4 h; ii) R_3-(C_6H_5)-CH_2-Cl or R_3-(C_6H_5)-CH_2-Br, Cs_2CO_3, DMF, 12 h; b) i) R_2-CO-Cl, DIPEA, DCM, 15 min; ii) 10% KOH in MeOH, 80 ^oC, 5 h; iii) R_1-OH, EDC, DMAP, DCM, 12 h or R_1-NH_2, DIPEA, PyBop, DCM, 12 h

Scheme 2. Synthesis of quinoline derivatives.

a) $POCl_3$, 1,2-DCE, reflux, 80 ^oC, 12 h; b) $SnCl_2$, EtOH, argon gas, 80 ^oC, 4 h; c) R_2-CO-Cl, DIPEA, DCM, 15 min; d) i) R_4-$B(OH)_2$, 2 M Na_2CO_3, $Pd(PPh_3)_4$, 1,4-dioxane, reflux, 80 ^oC, 3 h; ii) $SnCl_2$, EtOH, argon gas, 4 h; iii) CH_3I, DMF, 1 h; iv) 1.0 M LAH in THF, THF, 9 h

Table 1. P2X7R antagonistic activities of derivatives with modifications of quinolinone skeleton

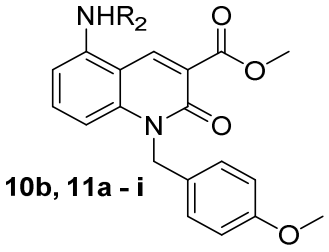

Compound	R_2	EtBr uptake in *h*P2X7-expressing HEK293 cells		
		% inhibition		
		10 μM	1 μM	IC_{50} (nM)[a]
1 (KN-62)		88 ± 2	79 ± 1	158 ± 18
2 (AZD9056)		97 ± 1	93 ± 2	2 ± 1
10b	H	NA.	ND.	ND.
11a	Ph-$(CH_2)_2CO$	56 ± 4	36 ± 3	ND.
11b	Ph-CH_2CO	43 ± 2	24 ± 2	ND.
11c	Ph-CO	NA.	ND.	ND.
11d	Cyclopentyl-$(CH_2)_2CO$	45 ± 2	15 ± 3	ND.
11e	Cyclohexyl-$(CH_2)_2CO$	57 ± 3	20 ± 3	ND.
11f	Cyclohexyl-CH_2CO	86 ± 3	63 ± 2	875 ± 15
11g	Cyclohexyl-CO	88 ± 2	67 ± 1	810 ± 12
11h	Adamantyl-CH_2CO	76 ± 1	65 ± 3	861 ± 10
11i	Adamantyl-CO	87 ± 2	76 ± 3	120 ± 50

NA. = No activity. ND. = Not determinded. [a]IC_{50} = 50% inhibitory concentrations were obtained from concentration–response curves. Data values are expressed as means ± SD. All experiments were repeated at least 3–6 times.

Table 2. P2X7R antagonistic activities of derivatives with modifications of quinolinone skeleton

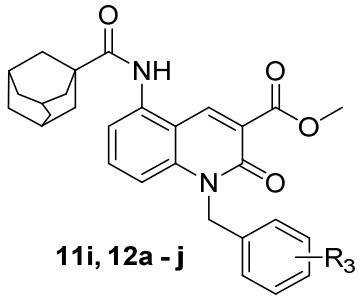

Compound	R_3	EtBr uptake in *h*P2X7-expressing HEK293 cells		
		% inhibition		
		10 μM	1 μM	IC_{50} (nM)[a]
1 (KN-62)		88 ± 2	79 ± 1	158 ± 18
2 (AZD9056)		97 ± 1	93 ± 2	2 ± 1
11i	4-OCH_3	87 ± 2	76 ± 3	120 ± 50
12a	3-OCH_3	55 ± 4	35 ± 2	ND.
12b	4-OCF_3	68 ± 3	48 ± 5	ND.
12c	4-F	86 ± 3	66 ± 2	888 ± 10
12d	4-Cl	88 ± 1	78 ± 3	723 ± 12
12e	4-Br	80 ± 4	65 ± 3	810 ± 10
12f	4-CH_3	45 ± 4	30 ± 5	ND.
12g	4-CH_2CH_3	38 ± 3	28 ± 3	ND.
12h	4-NO_2	85 ± 4	61 ± 2	809 ± 17
12i	4-CN	NA.	ND.	ND.
12j	H	NA.	ND.	ND.

NA. = No activity. ND. = Not determinded. [a]IC_{50} = 50% inhibitory concentrations were obtained from concentration–response curves. Data values are expressed as means ± SD. All experiments were repeated at least 3–6 times.

Table 3. P2X7R antagonistic activities of derivatives with modifications of quinolinone skeleton

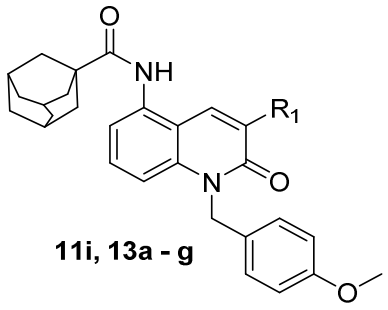

11i, 13a - g

Compound	R_1	EtBr uptake in *h*P2X7-expressing HEK293 cells		
		% inhibition		
		10 μM	1 μM	IC_{50} (nM)[a]
1 (KN-62)		88 ± 2	79 ± 1	158 ± 18
2 (AZD9056)		97 ± 1	93 ± 2	2 ± 1
11i	CO_2CH_3	87 ± 2	76 ± 3	120 ± 50
13a	H	43 ± 2	29 ± 1	ND.
13b	CO_2H	41 ± 1	2 ± 1	ND.
13c	$CO_2CH_2CH_3$	88 ± 2	86 ± 1	62 ± 10
13d	$CO_2(CH_2)_2CH_3$	87 ± 3	82 ± 3	263 ± 24
13e	$CO_2CH(CH_3)_2$	77 ± 2	47 ± 2	ND.
13f	$CONHCH_3$	42 ± 3	6 ± 1	ND.
13g	$CON(CH_3)_2$	54 ± 1	14 ± 1	ND.

[a] IC_{50} = 50% inhibitory concentrations were obtained from concentration–response curves. Data values are expressed as means ± SD. All experiments were repeated at least 3–6 times.

Table 4. P2X7R antagonistic activities of derivatives with modifications of quinoline skeleton

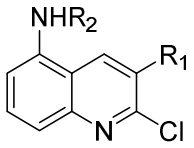

16a - e

Compound	R_1	R_2	EtBr uptake in *h*P2X7-expressing HEK293 cells			IL-1β release in differentiated THP-1 cells
			% inhibition		IC_{50} (nM)[a]	IC_{50} (nM)[a]
			10 μM	1 μM		
1 (KN-62)			88 ± 2	79 ± 1	158 ± 18	130 ± 20
2 (AZD9056)			97 ± 1	93 ± 2	2 ± 1	3 ± 1
16a	CO_2CH_3	Adamantyl-CH_2CO	43 ± 2	27 ± 12	ND.	ND.
16b	CO_2CH_3	Adamantyl-CO	21 ± 1	NA.	ND.	ND.
16c	H	Adamantyl-CH_2CO	97 ± 2	89 ± 3	4 ± 4	7 ± 2
16d	H	Adamantyl-CO	51 ± 3	11 ± 5	ND.	ND.
16e	H	Cyclohexyl-CH_2CO	95± 2	90 ± 2	385 ± 50	335 ± 12

[a]IC_{50} = 50% inhibitory concentrations were obtained from concentration–response curve s. NA. = No activity. ND. = Not determined. Data values are expressed as means ± SD. All experiments were repeated at least 3–6 times.

Table 5. P2X7R antagonistic activities of derivatives with modifications of quinoline skeleton

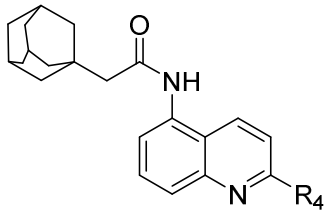

16c, 17a - k

Compound	R_4	EtBr uptake in *h*P2X7-expressing HEK293 cells			IL-1β release in differentiated THP-1 cells
		% inhibition		IC_{50} (nM)[a]	IC_{50} (nM)[a]
		10 μM	1 μM		
1 (KN-62)		88 ± 2	79 ± 1	158 ± 18	130 ± 20
2 (AZD9056)		97 ± 1	93 ± 2	2 ± 1	3 ± 1
16c	Cl	97 ± 2	89 ± 3	4 ± 4	7 ± 2
17a	Ph	86 ± 2	78 ± 2	447 ± 25	434 ± 10
17b	Ph-(4-OCH_3)	97 ± 1	89 ± 3	18 ± 2	29 ± 8
17c	Ph-(4-OH)	95 ± 3	79 ± 4	8 ± 3	6 ± 3
17d	Ph-(3-OH)	66 ± 4	36 ± 7	ND.	ND.
17e	Ph-(2-OH)	69 ± 2	41 ± 7	ND.	ND.
17f	Ph-(4-Cl)	90 ± 3	89 ± 3	123 ± 10	178 ± 13
17g	Ph-(4-NO_2)	94 ± 2	79 ± 3	73 ± 4	113 ± 8
17h	Ph-(4-NH_2)	93 ± 4	85 ± 3	10 ± 4	19 ± 3
17i	Ph-(4-CO_2H)	93 ± 2	87 ± 2	8 ± 2	25 ± 3
17j	Ph-(4-CO_2CH_3)	95 ± 1	90 ± 3	7 ± 3	33 ± 4
17k	Ph-(4-CH_2OH)	98 ± 2	95 ± 4	3 ± 2	12 ± 1

[a]IC_{50} = 50% inhibitory concentrations were obtained from concentration–response curv es. ND. = Not determined. Data values are expressed as means ± SD. All experiments were

repeated at least 3–6 times.

Table 6. Inhibition of human receptor subtypes P2X1-P2X4 by selected compounds

Compound	IC_{50} (μM) or % inhibition at 1 μM [literature data for comparison]			
	P2X1R	**P2X2R**	**P2X3R**	**P2X4R**
suramin	4.3 ± 0.8 [4.7][a]	ND.	ND.	ND.
PSB-1011	ND.	0.69 ± 0.15 [0.57][b]	ND.	3 ± 10%[c]
NF110	ND.	ND.	1.6 ± 0.3 [0.5][d]	ND.
5-BDBD	ND.	ND.	ND.	0.35 ± 0.08 [0.50][e]
16c	13 ± 2%	7 ± 1%	NA.	4 ± 5%
17b	25 ± 5%	3 ± 3%	3.0 ± 0.8	17 ± 2%

[a]Determined in rat vas deferens, using 10 μM αβmeATP as an agonist.[47] [b]Value obtained by two-electrode voltage-clamp electrophysiology in Xenopus oocytes transiently expressing the rat P2X2 receptor.[48] [c]Percent inhibition at 10 μM. [d]Endogenous rat P2X3 receptors in DRG neurons using the patch-clamp assay.[49] [e]Human P2X4 receptors expressed in Chinese hamster ovary cells.[50]

Table 7. Concentration of compound **16c** (ng/mL or ng/g) and brain/blood ratio in adult male zebrafish (n = 3, mean ± SD)

Time (h)	Matrix		T/P ratio
	Blood	Brain	
0.5	235 ± 112	425 ± 126	2.03

Table 8. BBB-PAMPA assay

(1) Solubility test (PAMPA buffer system)

Test concentration	Compound			
	17c	**17i**	**17k**	**17h**
50 μM	-	-	-	-
25 μM	-	-	-	-
12.5 μM	-	-	-	-

degree of precipitation: +++> ++ > +, (-) no precipitation.

(2) PAMPA

Compound	Concentration	Incubation time	P_e (10^{-6} cm/sec)	BCS code	Method
Progesterone	50 μM	4 h	36.552	High (CNS+)	U.V
Theophylline	50 μM	4 h	0.06	Low (CNS-)	U.V
17c	50 μM	4 h	16.441	High (CNS+)	U.V
17i	50 μM	4 h	8.463	High (CNS-)	U.V
17k	50 μM	4 h	17.671	High (CNS+)	U.V
17h	50 μM	4 h	24.855	High (CNS+)	U.V

(3) PAMPA: individual data

Compound	P_e (10^{-6} cm/sec)				
	1 st	2 nd	3 rd	mean	stdev
Progesterone	37.218	35.716	36.723	36.552	0.765
Theophylline	0.051	0.075	0.054	0.06	0.013
17c	17.784	15.698	15.84	16.441	1.166
17i	8.467	8.546	8.375	8.441	0.087
17k	18.159	16.934	17.921	17.671	0.650
17h	23.481	26.431	24.654	24.855	1.485

<Classification>

Permeability classification		CNS+/- classification	
P_e (10^{-6} cm/sec)	Classification	P_e (10^{-6} cm/sec)	Classification
> 0.4	High	> 10	+
< 0.4	Low	< 10	-

Table 9. *In-vitro* metabolic stability, Solubility and Permeability

(1) *In-vitro* metabolic stability (% of remaining after 30 min)

Compounds (1 μM)	Mouse (%)	Rat (%)	Human (%)
Verapami	-	-	10.5
16c	0.10	0.06	0.04
17c	14.5	12.9	21.5
17i	8.1	10.9	40.5
17k	17.0	11.2	17.9
17h	13.3	10.6	15.5

(2) Solubility and Permeability

	Method[51]	Compounds	Data	Comment
Solubility (Kinetic)	Nephelostar Nephelometry	**16c**	314.6 ± 2.9 μM (110.7 ± 1.1 μg/mL)	soluble or fairly soluble
Solubility (Equilibrium)	μSOL μSOL solubility program	**16c**	15.6 ± 0.568 μM (5.48 ± 0.200 μg/mL)	
		AZD9056	> 495 μM (> 207.4 μg/mL)	
Permeability	PAMPA	**16c**	-4.36	High: > -4.07 Medium: > -4.07~ -4.87 Low: < -4.87
		17c	-4.78	
		17i	-5.07	
		17k	-4.75	
		17h	-4.60	

Figure 1.

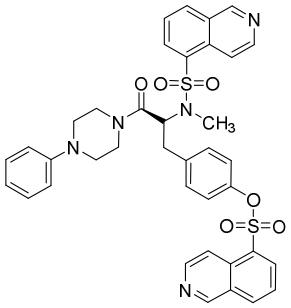

1, KN-62
(*h*P2X7, IC_{50} = 158 nM)

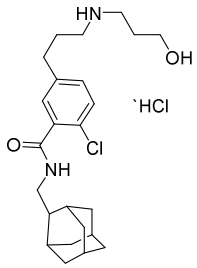

2, AZD9056
(*h*P2X7, IC_{50} = 1.5 nM)

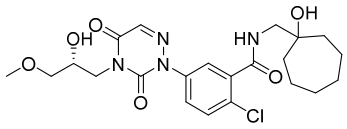

3, CE-224535
(*h*P2X7, IC_{50} = 4 nM)

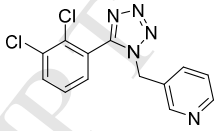

4, A-438079
(*h*P2X7, IC_{50} = 300 nM)

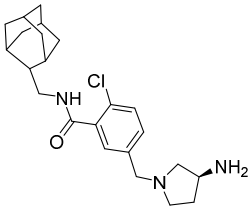

5. GSK314181A
(*h*P2X7, IC_{50} = 85 nM)

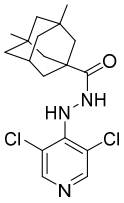

6
(*h*P2X7, IC_{50} = 13 nM)

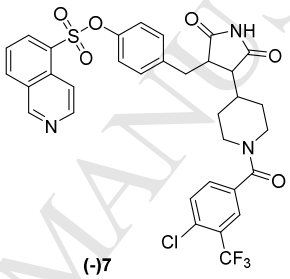

(-)7
(*h*P2X7, IC_{50} = 54 nM)

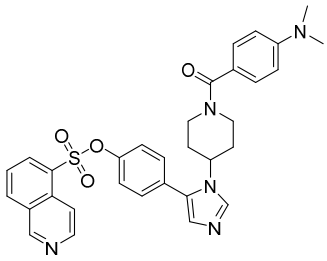

8
(*h*P2X7, IC_{50} = 0.11 nM)

Figure 2.

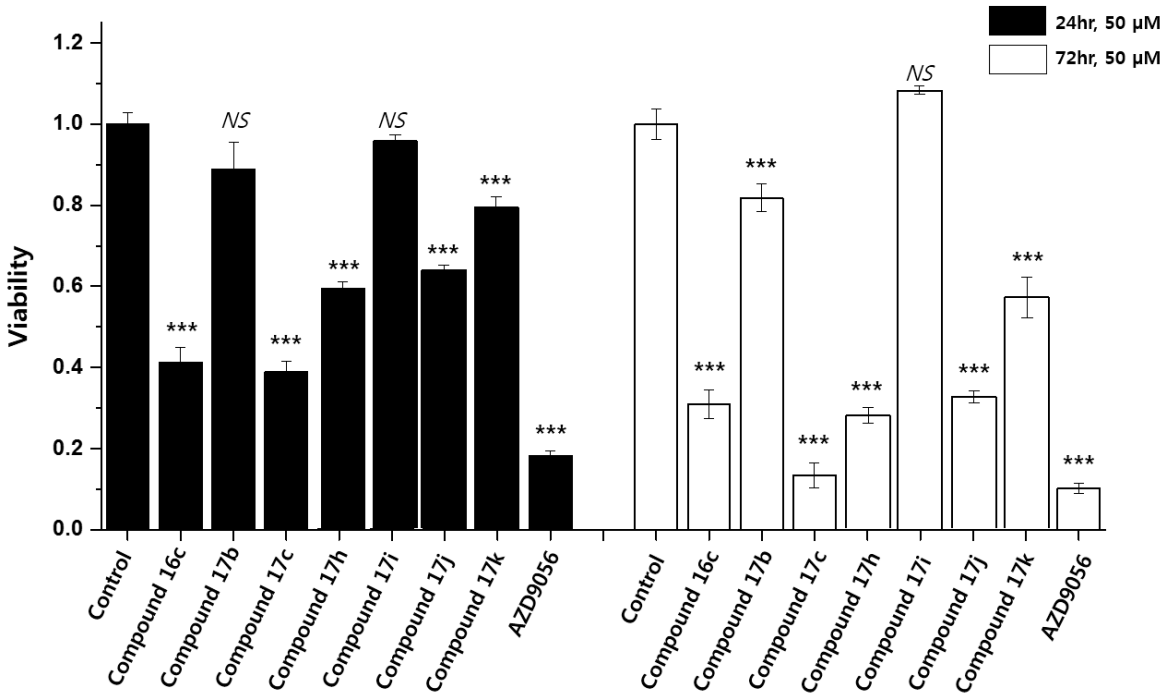

Figure 3.

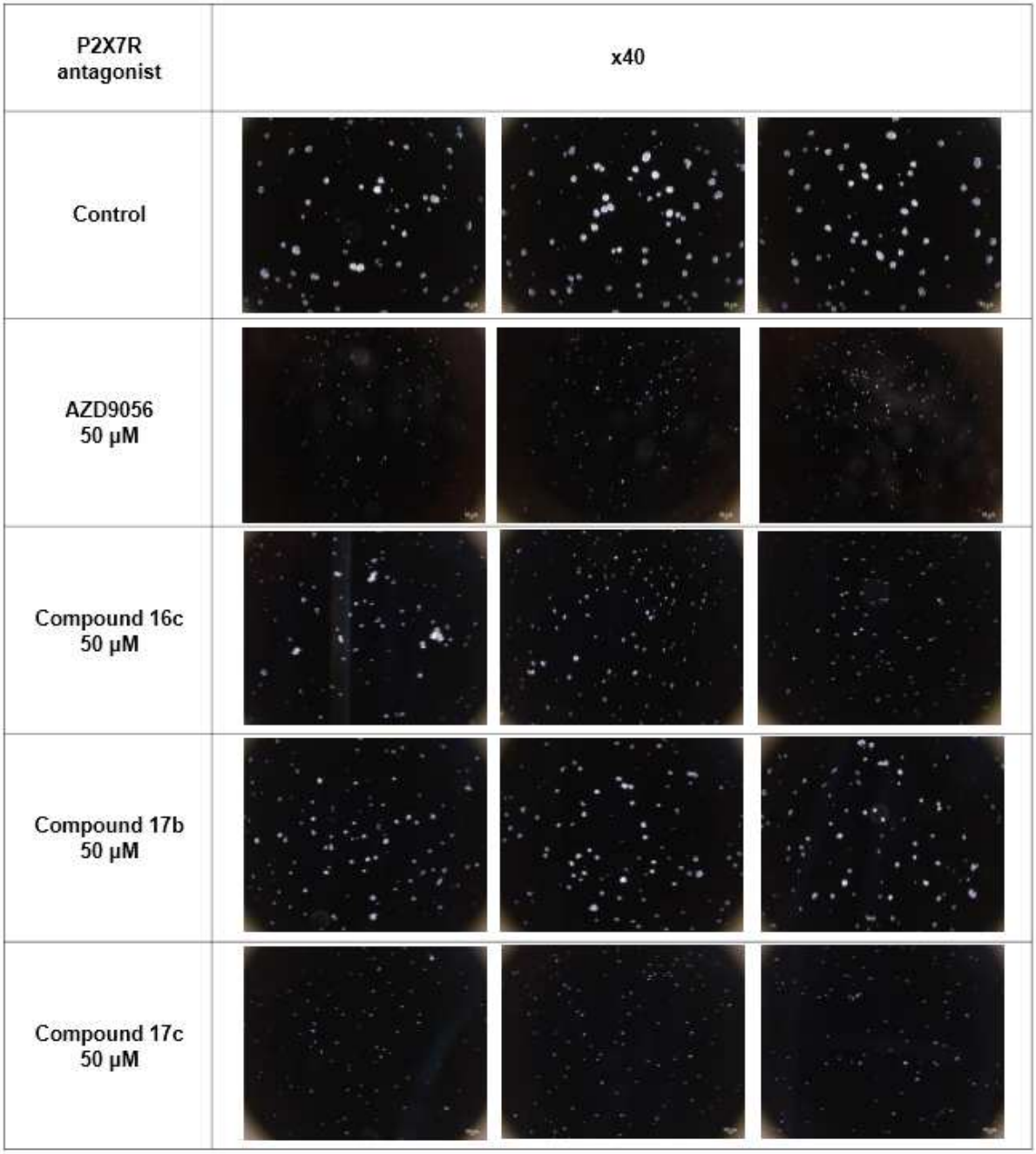
P2X7R antagonist
x40
Control
AZD9056 50 µM
Compound 16c 50 µM
Compound 17b 50 µM
Compound 17c 50 µM

P2X7R antagonist	x40
Compound 17h 50 µM	
Compound 17i 50 µM	
Compound 17j 50 µM	
Compound 17k 50 µM	

Figure 4.

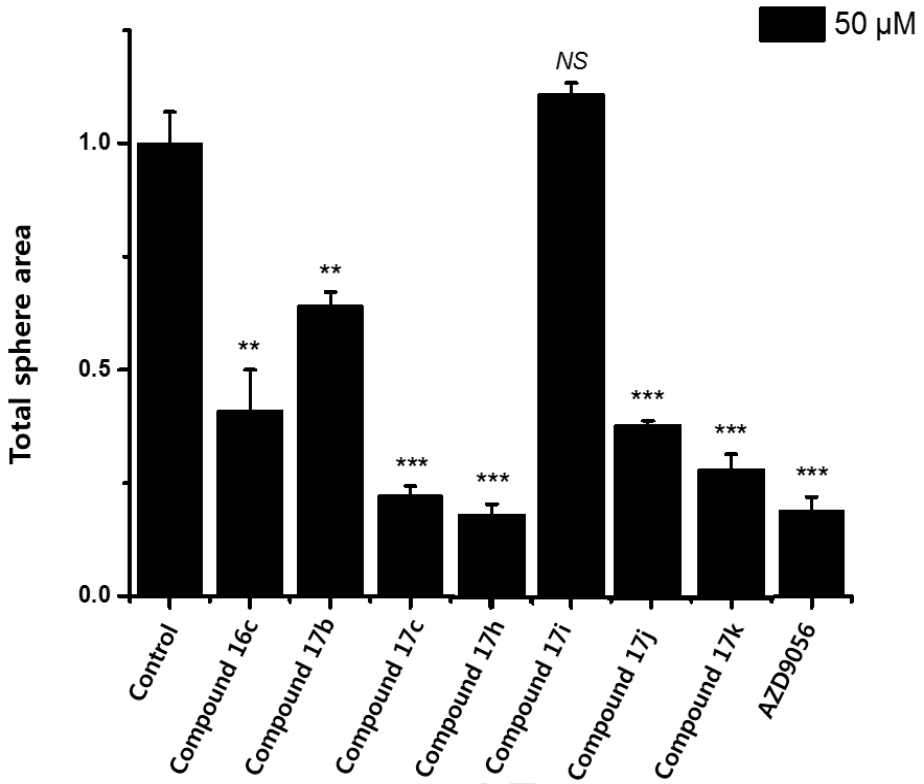

Figure 5.

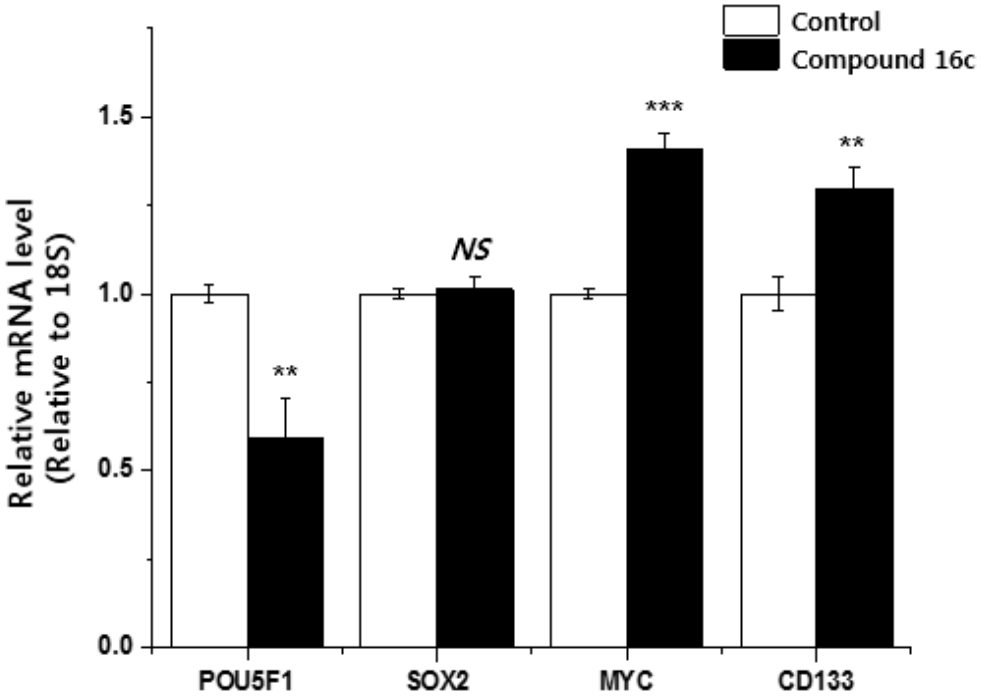

Figure 6.

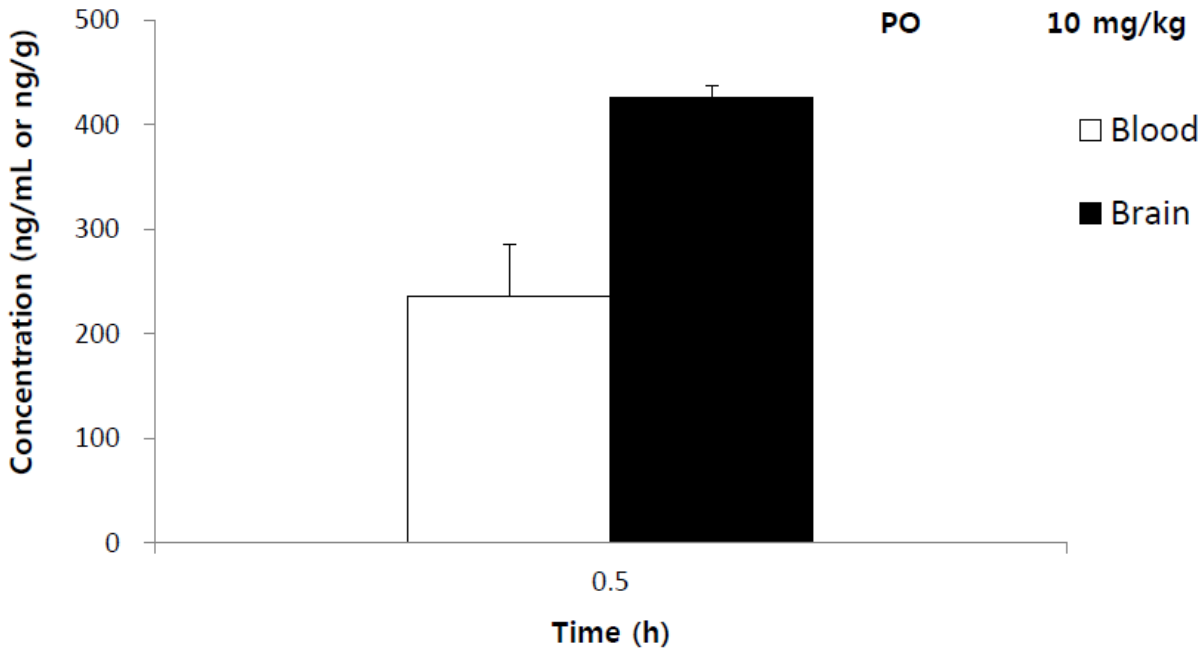

Scheme 1.

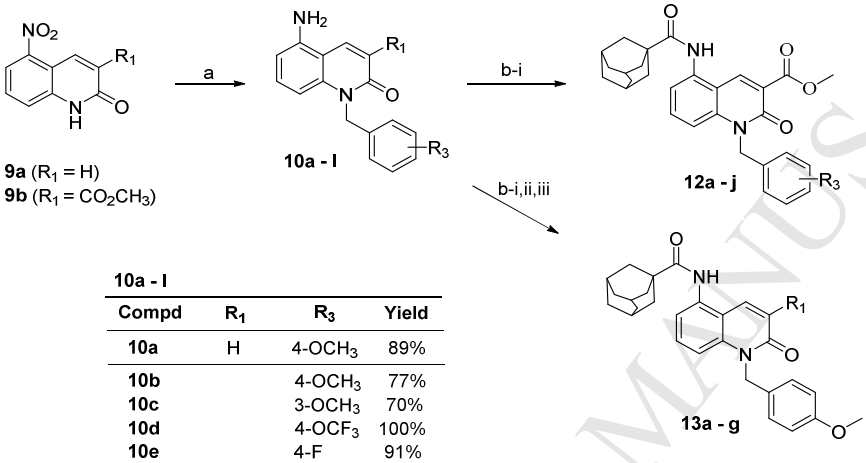

9a (R_1 = H)
9b (R_1 = CO_2CH_3)

10a - l

Compd	R_1	R_3	Yield
10a	H	4-OCH_3	89%
10b	CO_2CH_3	4-OCH_3	77%
10c		3-OCH_3	70%
10d		4-OCF_3	100%
10e		4-F	91%
10f		4-Cl	76%
10g		4-Br	77%
10h		4-CH_3	100%
10i		4-CH_2CH_3	89%
10j		4-NO_2	96%
10k		4-CN	78%
10l		H	87%

11a - i

Compd	R_2	Yield
11a	Ph-$(CH_2)_2CO$	35%
11b	Ph-CH_2CO	30%
11c	Ph-CO	39%
11d	Cyclopentyl-$CH(CH_2)_2CO$	37%
11e	Cyclohexyl-$(CH_2)_2CO$	36%
11f	Cyclohexyl-CH_2CO	37%
11g	Cyclohexyl-CO	17%
11h	Adamantyl-CH_2CO	33%
11i	Adamantyl-CO	27%

12a - j

Compd	R_3	Yield
12a	3-OCH_3	27%
12b	4-OCF_3	28%
12c	4-F	34%
12d	4-Cl	34%
12e	4-Br	36%
12f	4-CH_3	34%
12g	4-CH_2CH_3	27%
12h	4-NO_2	27%
12i	4-CN	26%
12j	H	22%

13a - g

Compd	R_1	Yield
13a	H	45%
13b	CO_2H	100%
13c	$CO_2CH_2CH_3$	38%
13d	$CO_2(CH_2)_2CH_3$	18%
13e	$CO_2CH(CH_3)_2$	37%
13f	$CONHCH_3$	20%
13g	$CON(CH_3)_2$	38%

Scheme 2.

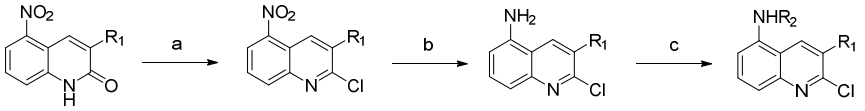

9a (R_1 = H)
9b (R_1 = CO_2CH_3)

14a (R_1 = H), y=75%
14b (R_1 = CO_2CH_3), y=82%

15a (R_1 = H), y=100%
15b (R_1 = CO_2CH_3), y=100%

16a - e

d

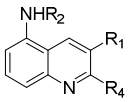

17a - k

16a - e

Compd	R_1	R_2	Yield
16a	CO_2CH_3	Adamantyl-CH_2CO	48%
16b		Adamantyl-CO	48%
16c	H	Adamantyl-CH_2CO	37%
16d		Adamantyl-CO	44%
16e		Cyclohexyl-CH_2CO	33%

17a - k (R_1 = H, R_2 = Adamantyl-CH_2CO)

Compd	R_4	Yield
17a	Ph	54%
17b	Ph-(4-OCH_3)	51%
17c	Ph-(4-OH)	34%
17d	Ph-(3-OH)	34%
17e	Ph-(2-OH)	34%
17f	Ph-(4-Cl)	49%
17g	Ph-(4-NO_2)	48%
17h	Ph-(4-NH_2)	30%
17i	Ph-(4-CO_2H)	40%
17j	Ph-(4-CO_2CH_3)	53%
17k	Ph-(4-CH_2OH)	15%

Highlights

- Quinoline derivatives were developed as P2X7 receptor antagonists.
- We performed the introduction of various substituents at the R_3 position of the quinoline structure.
- Compounds **16c**, **17b−c** and **17h−k** showed potent antagonistic effects (EtBr IC_{50} = 3-18 nM).
- Also, compounds **16c**, **17b−c** and **17h−k** exhibited highly potent functional activities (IL-1β IC_{50} = 7-33 nM).
- A representative compound **16c** has an acceptable *in vitro* anti-cancer activities against the glioblastoma cells, in which P2X7R receptors are overexpressed.